A MINIMAL CONSERVED REGION OF SHROOM2 AND SHROOM3 MEDIATES ACTIN BINDING AND BUNDLING

by

Hillary C. Cleveland-Rubeor

B.A., Bryn Mawr College, 2010

Submitted to the Graduate Faculty of the

Kenneth P. Dietrich School of Arts and Sciences in partial fulfillment

of the requirements for the degree of

Master of Science

University of Pittsburgh

2016

UNIVERSITY OF PITTSBURGH

KENNETH P. DIETRICH SCHOOL OF ARTS AND SCIENCES

This thesis was presented

by

Hillary C. Cleveland-Rubeor

It was defended on

May 26th, 2016

and approved by

Anthony Schwacha, Ph.D., Associate Professor, Biological Sciences

Jon Boyle, Ph.D., Associate Professor, Biological Sciences

Andrea Berman, Ph.D., Assistant Professor, Biological Sciences

Thesis Director: Jeffry Hildebrand, Ph.D., Associate Professor, Biological Sciences

A MINIMAL CONSERVED REGION OF SHROOM2 AND SHROOM3 MEDIATES ACTIN BINDING AND BUNDLING

Hillary C. Cleveland-Rubeor, M.S.

University of Pittsburgh, 2016

Changes in cell morphology are essential for generating the complex tissues that make up all organisms. Regulation of the cell's morphology is dynamic and is achieved through the coordinated activity of numerous signaling pathways and proteins that converge on the cytoskeleton at many levels. In epithelial cells, the Shroom family of proteins drives anisotropic changes to morphology such as apical constriction and convergent extension in the formation of such structures as the neural tube, vasculature, gut, and eye. Shroom proteins are a class of actin-binding proteins that recruit Rho-associated coiled-coil Kinase (or Rock), to the cytoskeleton to induce contraction of the actin network and effect change. Recent work in this field has focused on understanding the direct interaction of Shroom and Rock, but little work has been done to understand how Shroom proteins directly interact with actin. The actin-binding ability of these proteins has been localized to Shroom Domain 1, a domain unique to Shroom proteins. My work has centered on better understanding the interaction between the SD1 and actin.

I have identified small, conserved regions of both Shroom2 and Shroom3 that are capable of binding and bundling actin with similar affinity. With the use of Transmission Electron Microscopy, I observed that both proteins organize actin filaments into similar tightly packed parallel or anti-parallel bundles. While Shroom proteins localize to different populations of actin within the cell, it appears that the ability to bind and bundle actin has been conserved, and that other region of the proteins must drive their unique localization patterns.

TABLE OF CONTENTS

LIST OF TABLES

LIST OF FIGURES

LIST OF EQUATIONS

PREFACE

I would not have been able to accomplish this work without a lot of help and support from the people around me. First and foremost, I have to thank Jeff for being the best advisor a grad student could ask for. The sarcasm signs on your door let me know this was going to be a good fit from the beginning. Thank you for letting me figure it out as I went. I really need to thank you for letting me transition to this project after 2nd year. I have loved working on this project so much. Getting to try so many different techniques and pursue a more visual project was really great for me. Thank you for letting me help teach the new Shroom lab. But most of all, I have to thank you for being so supportive as I made this transition out of academia. It was very hard to make the decision to leave, but your support and understanding has made it much more manageable.

Thank you to the whole VanDemark Lab, past and present members, for all your contributions to my work in grad school. Thanks Andy for all your input and insight on my project. Thank you Jenna for putting up with me pestering you with questions on a daily basis. Thanks for being my compatriot on Team Shroom/Rock. You are an incredibly smart and hard working grad student, and I know you will do amazing things here and elsewhere once you have that shiny, well-earned Ph.D.. To Ryan and Josh, thanks for helping me troubleshoot so many protein purifications and making me laugh on a regular basis. Good luck in medical school guys!

So many people in this department have helped me become the scientist I am today. Thank you committee members: Tony, Andrea, and Jon. Your support and input during committee meetings was incredibly helpful. Also thank you for being so understanding and supportive of my decision to pursue a Masters. I feel incredibly lucky to have worked with all of you. I especially need to thank Andrea. I don't know if I would have been as successful in my first year of grad school without you. Working in your lab taught me how to be a grad student and not a tech. Thank you for helping me set up my third rotation and helping me find a lab home that was going to be a good fit. Thanks for being there for me during some of the hardest times I've seen in grad school. Thank you Debbie Chapman for all the baked goods, baking discussions, and snarky sarcastic conversations. You have inspired me to be a better, more adventurous baker. I also need to thank Bob Duda especially. Thank you for taking the time to teach me about TEM, showing me your awesome technique for making negative-stained grids, letting me borrow numerous reagents, and providing so much insight and encouragement as I ventured into new techniques with my projects.

Thank you to all the grad students in this department. Stay supportive of each other. Grad school is a challenge unlike any other, and everyone needs a support network. Don't forget to get out and see the sun sometimes. A Ph.D. is great, but what will you do with it if you are burnt out and hate everything? Don't forget to stop and realize all that you have accomplished. We as grad students often slip into a place of doubt and judgment of ourselves and our work because we have to be so introspective all the time. Don't forget that what you are doing is amazing. Don't get too jaded. Thank you to anyone who ever invited me out to something. Thanks for the happy hour drinks, game nights, movie nights, skating, hanging out, or even just chatting in the hall while I made laps of Langley 3rd to stretch my legs, thaw my hands, and make tea.

Thanks to my classmates, especially Dominique and Elizabeth. I have way too many things to thank you guys for, but I'll say this: thanks for listening and thanks for talking. Thanks for listening to me talk through everything that was going on, good or bad. Thanks for trusting me to share what was going on for you. I may be moving across the country, but I am only a text/phone call/message away. I'm always here to listen. Do what you need to do for you, whatever that is.

While my graduate career has been shaped and molded by the people in the department, I have many more people in my life I need to thank. Thank you Mom and Dad for letting me stay up past my bedtime when I was a little girl to watch *NOVA* and *Nature*. Thanks for letting me play with a microscope, taking me to science museums all the time, and nurturing my love of art at the same time. Thank you for not pigeonholing me and letting me develop these two loves of science and visual art. Thank you to my big brother, Aaron, for being there for the random phone calls and all of the career advice. I can't wait to live closer to you in the Northwest. Thanks to the rest of my family for being there for me. I love you all. Thank you Rubeor clan for making me a part of your family. I am so touched by how you have welcomed me into your lives. Thank you for all your support and advice. Thank you to all the animals in my life during grad school. Thank you to my family dogs. Rest in peace Luke, and I love you Charlotte.

I have saved the most important person for last. Without you, my darling, I very literally wouldn't have reached this day. I don't know if there is really something like fate in the world, but if there isn't, it is one hell of a coincidence that we both ended up in Pittsburgh at the same time. You are my world. You are the confidence I needed to leave my old job and pursue grad school. You never let me settle for just ok. You pushed me to realize my dreams. Thank you is not sufficient. I love you.

1.0 INTRODUCTION

1.1 CELL MORPHOLOGY AND THE NEURAL TUBE

In order for complex structures and organs to form in a developing embryo, drastic changes must occur to cell morphology. These include changes to cell shape, size, location, and fate and all are controlled or modified through complex interactions of regulatory pathways and the cytoskeleton. Many of these pathways, at their most basic level, are involved in the rearrangement of the actomyosin network in epithelial cells. One example of a pathway involved in these rearrangements of the actomyosin network is the Planar Cell Polarity (PCP) pathway [1, 2]. This pathway helps to regulate the anisotropic changes to cell morphology that drive the formation of such structures as the neural tube [3-5]. When we think of anisotropic changes to cell morphology, we can think of two particular examples involved in the formation of the neural tube: apical constriction and convergent extension (Fig. 1.1). Apical constriction is the process by which cells specifically constrict on their apical surface, while their basal side remains relatively unchanged [6]. This transformation from a columnar to a wedge shape allows flat sheets of cells to transform into curved tissues. Apical constriction is apparent in the development of the neural tube, but also in other structures such as the eye [7, 8].

Convergent extension, by comparison, is the process by which cells differentially contract mediolateral cell-cell borders and not anterior-posterior borders, leading to an

anisotropic change in cell morphology (Fig. 1.1 B & D) [2, 9]. By contracting in the mediolateral direction, cells can intercalate between each other. The cells converge as a rosette, and then extend in anterior-posterior direction. This extends a wide, short tissue into a long, narrow tissue without needing to increase the total number of cells. Convergent extension allows the developing embryo to extend its body axis [4]. The PCP pathway regulates the location of other pathways and helps to direct these localized anisotropic changes to cell morphology needed for tissue bending [2].

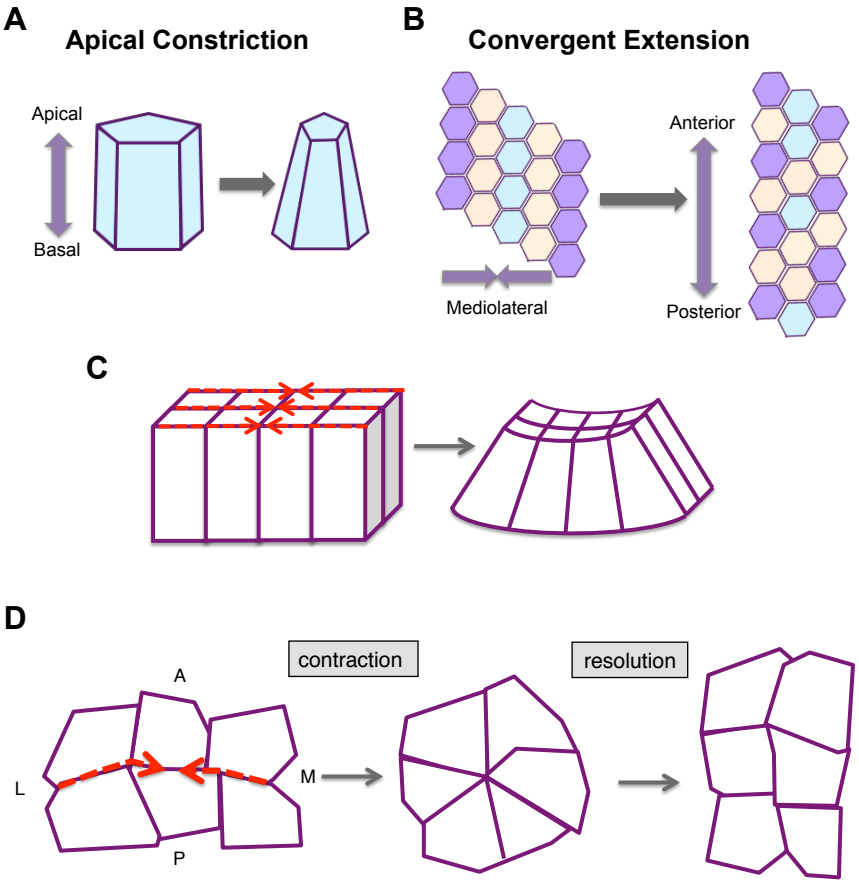

Figure 1.1: Changes to cell shape are critical to development.

Regulation of the actomyosin network of cells is at the center of A) apical constriction and B) convergent extension. These anisotropic changes to cell shape can be seen in the C) bending of tissue (apical constriction) and D) tissue extension (convergent extension) through rosette formation.

1.2 ACTIN

Actin is found in all metazoan cells. Actin and the other components of the cytoskeleton contribute to many aspects of dynamic cell behavior, such as cell shape change, migration, and transport of materials in the cell. Actin often works in complex with actin-binding proteins (ABPs), to regulate cellular responses to extracellular stimuli [10-18]. Actin is found in two states, monomeric globular (G) actin and filamentous (F) actin. G-actin is polymerized into F-actin in an ATP-assisted manner. G-actin can be added to either end of a filament, though it is more common to be added to the growing end known as the barbed end (or + end). At the other end, known as the pointed end (or – end) of the F-actin filament, G-actin monomers will spontaneously de-polymerize from the filament [15-17, 19, 20]. This cycling of G-actin to F-actin to G-actin creates a constant flux in the population of actin in the cell.

F-actin can be further organized into different arrays such as branched networks, bundled cables, and gel-like mesh [10, 13, 21-27]. These different architectures allow actin to play many different roles in a cell. For example, bundled parallel actin filaments, in the presence of myosin, can be contracted against each other to generate force that is critical to changing a cell's shape [18, 28, 29]. Branched networks of actin are critical to giving a cell rigidity, facilitating migration, and dictating the overall shape of the cell [19].

1.2.1 Actin Binding Proteins

While actin can do many things on its own, it also works in conjunction with numerous ABPs. Fig. 1.2 shows examples of the four classes of ABPs: A) polymerization regulators, B and C) architecture modifiers, D) translocation and force generation, and E) anchoring proteins. ABPs

are a complex group of proteins that employ a diverse range of binding sites and motifs to associate with actin. More than 18 different actin-binding motifs have been identified [22]. While some motifs can be found across several actin-binding proteins, such as the C2 domain found in Protein Kinase C-delta and Fragmin60, others are more specialized to specific ABPs such as the actin-binding motifs of Myosin and Profilin [17, 22, 23, 30, 31]. Actin itself contains many different binding sites that ABPs use, adding to the diversity of interactions.

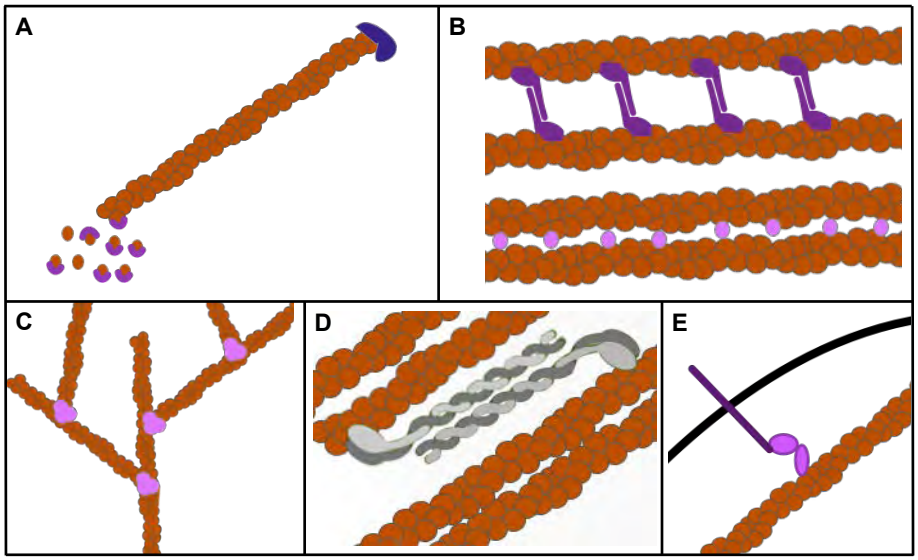

Figure 1.2: Four Classes Of Actin Binding Proteins.

A) Polymerization; Nucleation promoters (Profilin) and capping proteins (CapZ), B) F-actin architecture; bundling proteins (a-Actinin and Fimbrin), C) F-actin-architecture; branching networks (Arp2/3 complex, also a Nucleation Promoting Factor, NPF), D) Translocation; myosin, E) Anchoring actin; proteins that link actin to the cell membrane (Catinins linked to Cadherin). There is evidence to suggest that Shroom proteins exhibit activities consistent with more than one category of actin-binding protein.

1.2.1.1 Polymerization

Profilin and the Arp2/3 complex are two examples of ABPs that facilitate the nucleation (Arp2/3, Fig 1.2C) and growth (Profilin, Fig 1.2A) of F-actin [22, 32]. Profilin regulates the elongation of F-actin in several ways. Profilin binds G-actin and sequesters it from the available pool of G-actin available for spontaneous filament assembly [22, 27]. It helps catalyze the transition from ADP-actin to ATP-actin. ATP-actin is more readily polymerized than ADP-actin. Profilin also interacts with Ena/VASP proteins that promote the elongation of F-actin [22].

The Arp2/3 complex works by mimicking several G-actin monomers in the orientation of those in an F-actin filament. The Arp2/3 complex can bind the side of an F-actin filament and create a branch point in the filament. G-actin will be added now to both + ends, that of the original filament as well as the new branch. This creates a branched/mesh network, important in creating force and strength at the edge of a cell. The WAVE and WASP family of proteins work in conjunction with the Arp2/3 complex to help promote the polymerization of actin [11, 22, 33-38].

At the pointed end of the F-actin filament, capping proteins, such as CapZ (Fig 1.2A), bind to and stabilize the filament from depolymerizing. Stabilizing the F-actin makes the filaments more resistant to de-polymerization and degradation. Cofilin on the other hand actively de-polymerizes F-actin back into G-actin. Finally, there are proteins such as Gelsolin that cleave F-actin into small fragments. This group of actin-binding proteins are especially diverse and several of them play additional roles in regulating actin [22].

1.2.1.2 Architecture

The next group of ABPs are the architecture-modifying proteins (Fig 1.2 B and C). F-actin can adopt several different geometries in a cell, including bundles, branched filaments, and gel-like

networks. As mentioned above, the Arp2/3 complex helps to branch F-actin by binding the side of an F-actin filament (Fig 1.2C). The filament can now continue to polymerize in two directions [34, 36, 37]. Another ABP, Filamin, binds F-actin and creates networks of filaments at 90° angles to each other, creating a mesh. This mesh of actin commonly helps to create strength and rigidity at the cellular periphery [18, 27].

Bundles are formed when multiple F-actin filaments are brought together in either a parallel or anti-parallel orientation (Fig 1.2B). ABPs that crosslink actin filaments into bundles must have multiple actin-binding motifs [10, 13, 21, 23, 25, 26, 32, 39, 40]. Monomoers containing a single actin-binding motif must mulitmerize in order to bundle actin. α-Actinin and Villin are two examples of actin bundling proteins that dimerize. α-Actinin has a single actin-binding motif, however it dimerizes in an anti-parallel formation. This positions the actin-binding motifs approximately 30 nm apart, facilitating a loose actin bundle. This gap is sufficient for Myosin to fit between the F-actin filaments [26].

Villin is an interesting example of an ABP with unique properties and regulation. Unlike α-Actinin, Villin has two functionally different actin-binding motifs, one in the head domain and one in the core. The actin-binding motif of the head is solely for binding actin, while the one in the core of the protein is required for Ca^{2+}-dependent cleavage of F-actin. Villin can dimerize in a manner that blocks the core binding site. This allows the actin-binding motifs of the dimer to crosslink actin filaments. Villin induces a tighter actin bundle than that of α-Actinin, as it dimerizes in a parallel direction, which positions the actin-binding motifs close together [24, 40, 41].

Fimbrin is an example of an actin-binding protein that contains 2 actin-binding motifs in a single monomer. Due to Fimbrin's small size and the proximity of the two actin-binding

motifs, this positions the actin filaments in a bundle only ~5nm apart. The tighter packing of the F-actin bundle precludes myosin from interacting with the core of the bundle [21, 23, 25].

These differences among ABPs are prime examples of how actin can be modified in different ways to suit different requirements. A tight knit bundle will be inherently stronger than a single filament and is necessary for the generation of force required to change a cell's morphology [14, 18, 42]. More permanent structures such as those found in microvilli also require a denser actin bundle [24]. In contrast, deliberately spacing F-actin farther apart facilitates the interaction with myosin and contractile networks [18].

1.2.1.3 Translocation

The third group of ABPs corresponds to the myosin family of proteins which are involved in translocation (Fig. 1.2C). While Myosin is typically thought of in the context of muscle cells, it is a large family of proteins that play many different roles with in a cell [18, 28, 29, 43-45]. For example in non-muscle cells, non-muscle MyosinII (nmMyoII) is phosphorylated and translocates along the F-actin filament generating force and contraction of F-actin filaments. This generation of force is central to the changes in cell morphology described in section 1.1. nmMyoII can work on actin bundles as well as single F-actin filaments, helping to generate strong mechanical force on a cell [18, 28, 29, 46]. Directed force generation is necessary for the anisotropic changes to cell morphology.

Other members of the Myosin family, notably MyoV, are involved in the transport of cargo through the cell along F-actin. This cargo can consist of vesicles, RNAs, or even organelles. MyoV's motor component is different than that of MyoII, allowing it to "walk" along the actin filaments toward the minus end [43, 45].

1.2.1.4 Linking actin to the cell membrane

The last group of ABPs are those that link F-actin to the cell membrane (Fig. 1.2E). These proteins are typically multi-domain scaffold proteins that are capable of binding to ether membrane lipids or the cytoplasmic portions of transmembrane proteins and to F-actin. Particularly important are the connections of F-actin to cell-cell junction complexes. For example, α-Catenin forms a complex that binds actin and links it to E-cadherin at adherence junctions [47-50]. Actin associated with cell-cell junction, such as adherence junctions, is critical for changes to a tissue shape, consistent with its role in remodeling cellular architecture [48, 51, 52].

1.3 SHROOM/ROCK PATHWAY

The Shroom/Rock pathway rearranges the cellular cytoskeleton through directed contraction of the actin network [6, 53, 54]. Different Shroom family members are expressed in different cell types and localize to unique areas of cells, consistent with the involvement of Shroom proteins in the proper development of the nervous system, sensory cells, eyes, vasculature, and gut [55-62]. All Shroom proteins effect change on the actin cytoskeleton by recruiting Rock to the cytoskeleton (Fig. 1.3) [63]. Once there, Rock activates nmMyoII, which in turn contracts the actin network, changing the shape of a cell and its neighbors [53, 64-66].

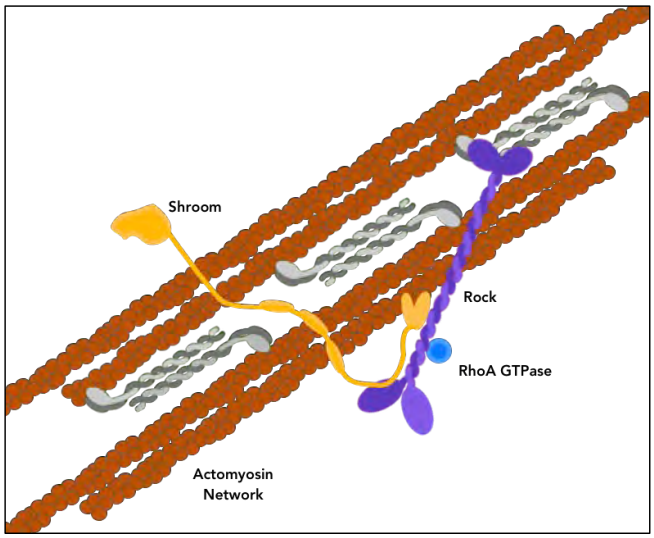

Figure 1.3: Working Hypothesis of the Shroom/Rock Pathway.

Conserved across the Shroom family of proteins is the ability to localize to actin and recruit Rock to the cytoskeleton. Our data suggests that Shroom can directly activate Rock, which in turn activates non-muscle Myosin II, leading to actin contraction.

1.3.1 The Shroom Family of Proteins

The Shroom family can be found in most metazoans, from *D. melanogaster* to Humans [60]. *Drosophila* only has 1 copy of Shroom in the genome, dShroom, however there are several splice-variants that encode full-length (dShroomA) and N-terminally truncated versions (dShroom B and C) of the protein [67]. In contrast, mammals having four separate *Shroom* genes, *Shroom1-4*, that encode proteins that all have unique localization characteristics (Fig. 1.4) and are involved in different roles in development [60, 68]. I will focus on the mammalian version of the Shroom proteins for the rest of this document unless otherwise indicated.

While each Shroom protein has a unique expression profile, there are several characteristic features that define the family (Fig. 1.5). They all contain a highly conserved C-

terminal Shroom Domain 2 (SD2) that binds to Rock and subsequently recruits it to the actomyosin network [6, 63, 69-72]. Most members of the family also contain a centrally located Shroom Domain 1 (SD1). The SD1 is generally considered the actin-binding region, though a definitive actin-binding motif has not yet been elucidated for the Shroom family [57, 60, 68, 69]. The SD1 is less highly conserved across the family than the SD2. Finally, most Shroom proteins contain an N-terminal PDZ domain [69, 73]. While there is an NMR structure of Shroom4's PDZ [73], there is no known function at this time for this domain in regards to Shroom activity. However, PDZ domains typically act as protein-protein interaction domains, suggesting that it may have a similar function for Shroom [74, 75].

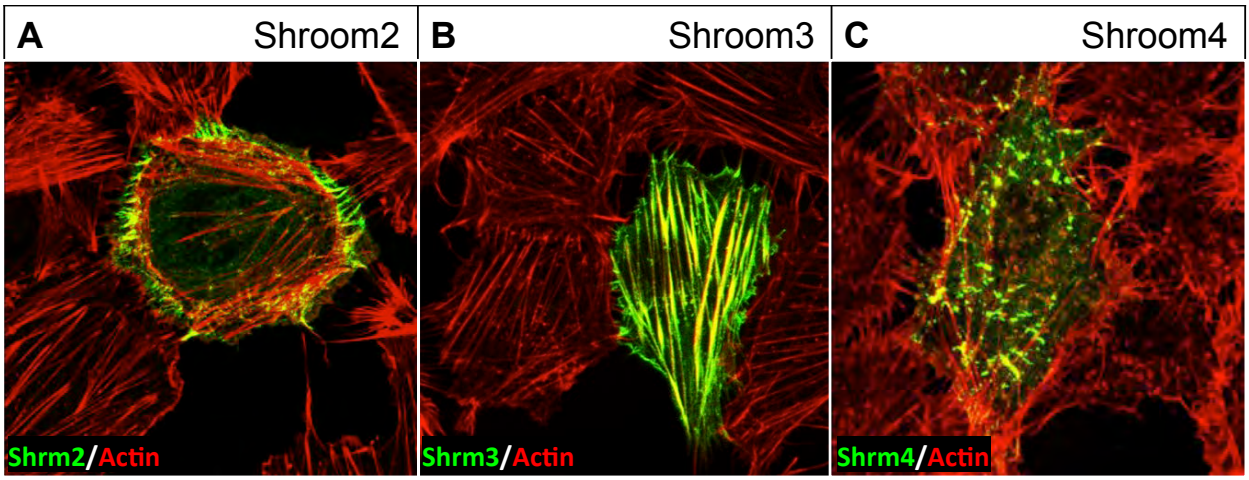

Figure 1.4: Differential localization of Shroom family members in Fibroblasts.

Rat Fibroblasts were transfected with expression vectors for Shroom2, Shroom3 or Shroom4 and stained to detect each protein. A) Shroom 2 localizes to cortical actin, B) Shroom3 localizes to actin stress fibers, C) Shroom4 localizes to cytosolic actin punctae. Figure modified from Dietz et al. 2006 [68].

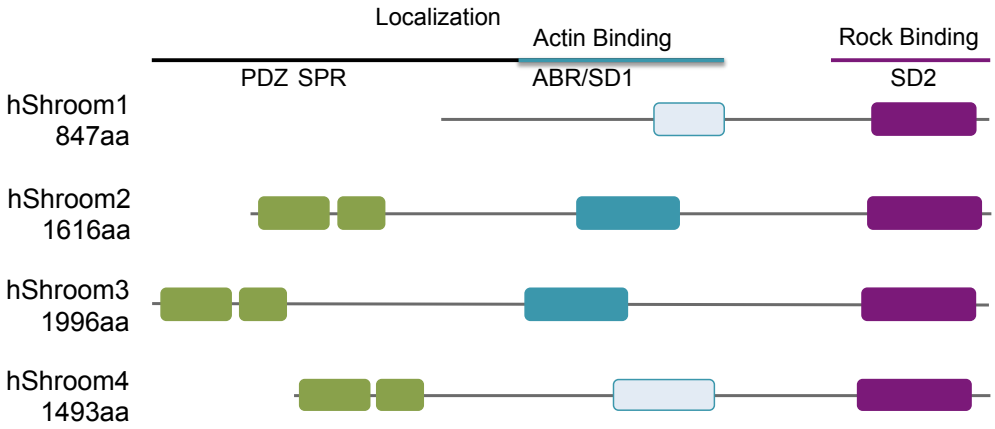

Figure 1.5: Domain map of the Shroom family of proteins.

The Shroom family contains several conserved domains: PDZ, Serine Proline Rich (SPR), SD1, and SD2. They vary in length as well as tissue expression and subcellular locations, during development and in adult tissues. Figure adapted from S. Mohan and J. Zalewski.

1.3.1.1 Shroom3

Shroom3 has been studied more extensively than other members of the Shroom family. It was first discovered in a mouse genomic screen looking for genes responsible for neural tube development [69]. Shroom3 was named for its phenotype; the neural tube in *Shroom3* mutant mice, mushrooms out instead of properly closing. While being the first protein to be named Shroom, it was found to be homologous to two other proteins already known to exist: Apical Protein Xenopus (APX), and APX Like (APXL) [69]. In the original study, Shroom3 was characterized as a PDZ containing, actin-binding protein [69]. Work from our lab and others further elucidated that Shroom3 localizes to the apical portion of cell-cell adhesion sites in epithelial cells to regulate apical constriction [6, 63]. Domain mapping studies of Shroom3 indicated that the SD1 and SD2 motifs are both required for apical constriction. These studies showed that the SD1 is required for localization to actin and the SD2 is required for recruiting

Rock [6, 68]. Shroom3 and Rock are critical not only for neural tube closure but also for the extension of the body axis through convergent extension of cell layers [2, 53, 63, 71, 72]. When Shroom3 is ectopically expressed in fibroblasts it localizes to actin stress fibers across the cell (Fig. 1.4B). Shroom3's SD1 has also been shown to co-sediment with F-actin in actin-binding experiments [69].

When we look at Shroom3 *in vivo*, Shroom3 directly interacts with components of other pathways important to regulating cell morphology in different cell types, helping to specialize its role in development [2, 8, 61, 63, 76]. Previous work from our lab has shown that Shroom3 co-localizes and co-sediments with the Dishevelled2 protein of the PCP pathway [2]. We believe this interaction helps to refine Shroom3 localization to the apical junctions of cells, where we know other members of the PCP pathway are located, such as Frizzled (Fig. 1.6A) [2]. In growing neurons, Shroom3 localizes to the base of axons and directly interacts with the Plenty of SH3 (POSH) protein (Fig. 1.6B). Once at the base of an axon, the Shroom3/Rock complex helps to regulate axonal outgrowth by inducing actin contraction within the axon [76, 77].

1.3.1.2 Shroom2

Shroom2 was originally classified as Apical Protein Xenopus Like, APXL, however it was renamed when the "Shroom" nomenclature was established [78]. Shroom2 is expressed in epithelial cells throughout the developing embryo, where it is involved in vasculature and gut morphogenesis, as well as in kidney development [59, 60, 68]. It can also be found in the sensory cells of the eyes (rods and cones) and inner ear (vestibular hair follicles) [57-59, 68]. Shroom2 contains the N-terminal PDZ, central SD1, and C-terminal SD2 typical of the Shroom family. The SD2 is competent to recruit Rock to the actomyosin network. Shroom2 is also an ABP with a conserved SD1 that co-sediments with F-actin [57]. Shroom2 functions in much the same

manner as Shroom3, however it is expressed in different tissues and localizes to different populations of actin. We have found that Shroom2 has a unique localization pattern when expressed in fibroblasts compared to Shroom3. Shroom2 localizes to cortical actin, where as Shroom3 localizes to actin stress fibers (Fig. 1.4A vs. B) [68]. One group has shown that Shroom2 directly interacts with ZO-1 and MyosinVIIa at adherens junctions (Fig. 1.6C) [57].

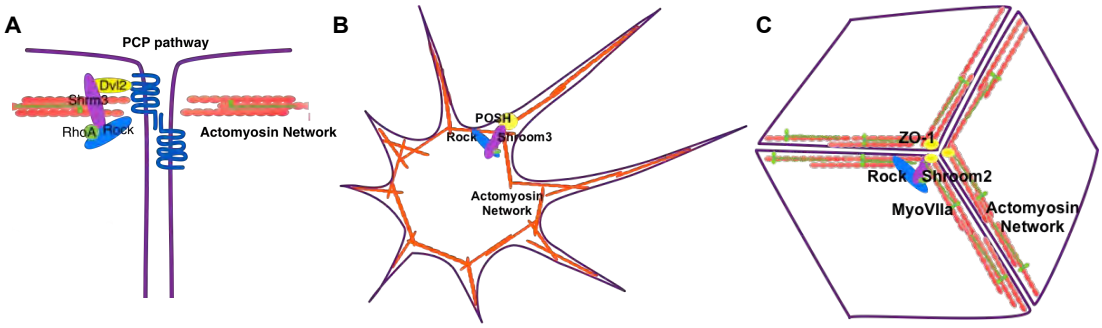

Figure 1.6: Shroom3 and Shroom2 localize differently with upstream proteins.

Specialization of the Shroom family members may be achieved though localization with other upstream pathways and proteins. A) Shroom3 localizes and binds to Dishevelled2 (Dvl2) of the PCP pathway [2]. B) Shroom3 also localizes to POSH in developing neurons [76]. C) Shrm2 localizes with and directly bind ZO-1 and MyosinVIIa in sensory cells such as inner ear hair follicles [57].

1.3.1.3 Shroom4

Shroom4 was originally designated as KIAA1202, but was later reclassified when the "Shroom" nomenclature was adopted [78]. It contains the N-terminal PDZ and C-terminal SD2, but it lacks a well-conserved SD1. There is some conservation between the central region of Shroom4, Shroom2 and Shroom3, though it is debatable if it truly has a complete SD1 [60, 78]. Shroom4 does localize with cytosolic actin punctate when expressed in fibroblasts, and can bind actin *in vitro* [62, 68]. It is unclear if Shroom4 induces the formation of the actin punctae or if it localizes

to actin architecture already found in the cell. Mutations in *SHROOM4* have been associated with X-linked mental retardation in humans [79].

1.3.1.4 Shroom1

Shroom1 is the least well studied member of the Shroom family. Although it has some similarities to Apical Protein *Xenopus* (APX), it is likely unique to mammals [60, 78]. Shroom1 is the smallest member of the vertebrate Shroom family at only ~850 amino acids. Shroom1 lacks the N-terminal PDZ domain that is shared among the other Shroom family members and it is debatable if it actually contains a complete SD1 [55, 60, 78]; the conservation of the central region is so low among the family members, it makes defining the SD1 difficult. This will be discussed in section 1.4.2 in more detail. Shroom1 does contain a putative SD2 motif, but it has not been shown to bind Rock [55].

1.3.2 Rho Associated Coiled-coil Kinase

Rock kinase activity is required for Shroom-induced change in cell morphology [53, 63]. Rock consists of 3 regions, an N-terminal Kinase domain, a central coiled-coil region, and a C-terminal PH/C1 domain [63-65, 72, 80]. Rock forms a parallel dimer through its core coiled-coil region, with the dimerization domain located C-terminal to the Kinase domain. N-terminal to the coiled-coil region, the 2 copies of the PH/C1 domains fold independently of each other [81]. Within the coiled-coil region are two known protein binding domains, the Shroom Binding Domain (SBD), which binds Shroom's SD2, and the RhoA Binding Domain (RBD), which binds the active form of the RhoA GTPase [65, 72, 80, 82-87]. While Rock has been shown to be

involved in actin regulation, it has never been shown that Rock directly associates with actin [64, 65, 88, 89]. Thus, to regulate cytoskeletal changes, Shroom must recuit Rock to actin.

1.4 SHROOM AND ACTIN

Beyond binding Rock, the Shroom family proteins bind F-actin. This characteristic has been understood since the identification of Shroom. The SD1 region is responsible for binding actin [6, 68, 69]. Work from our lab and others has narrowed down the boundaries of the SD1 region responsible for actin-binding, but the interaction is still poorly understood [6, 57, 60, 68, 69]. The scope of this work will focus on the SD1 domain and its interaction with actin.

1.4.1 Shroom's Role as an Actin Binding Protein

Since its characterization as a cytoskeletal protein, other aspects of Shroom's role as an ABP have been investigated. Based on these studies, Shroom appears to have multiple ABP roles (Fig. 1.2): First, Shroom has been shown to protect F-actin filaments in cells treated with Cytochalasin D treatment [68]. Cytochalasin D prevents the addition of new monomers to F-actin as well as preventing other ABPs binding to the barbed end. In this way Shroom plays a role in stabilizing filaments. Second, both Shroom2 and Shroom3 induces actin bundles *in vitro* [68] and Shroom3 recruits and reorganizes actin *in vivo*. When ectopically expressed and artificially targeted to the mitochondria, Shroom3 recruits actin to this location [6, 68]. This characterizes Shroom as having a role in reorganizing actin architecture on multiple levels. Third the Shroom/Rock pathway is directly responsible for phosphorylating nmMyoII, and thus leading to translocation

of myosin along the filaments [6, 53, 54, 63, 90]. Finally, Shroom2 and Shroom3 directly interact with and cell membrane proteins (Shroom2, ZO-1 at adherence junctions) [57] scaffolding proteins (Shroom3, Dishevelled which binds Frizzled) [2]. Additionally, the PDZ domain of Shroom could bind additional currently unknown membrane proteins, as other PDZ domains are known to do [74, 75]. These different roles position Shroom family proteins as unique and complex ABPs. Despite this information, we still do not know how Shroom is able to bind actin or effect changes in actin architecture.

1.4.2 SD1

Shroom proteins regulate actin directly through binding and bundling of the actin filaments and indirectly through recruitment of Rock and the activation of nmMyoII. Previous work has focused on the indirect effect on the cytoskeleton. This work is focused on the biochemistry of Shroom/actin binding. The SD1, as previously mentioned, is found in most Shroom family members. While we describe it as a domain, it does not follow traditional definitions of a domain; it lacks unique predicted secondary structure such as that observed in the PDZ domain, and it also lacks clear boundaries based on sequence conservation [69]. Additionally, initial limited proteolysis experiments have not revealed a stable domain (data not shown). However, the SD1 acts as an individual domain in that it can successfully bind actin independent of the other domains of Shroom [6, 68].

In an effort to better define the SD1, alignments of Shroom2, Shroom3 and Shroom4 were analyzed. It was found that there are patches of conservation between Shroom 2, 3, and 4, as well as regions unique to only 1 or 2 family members (Fig. 1.7). Given their conservation, it is possible that these patches of similarity contain sequences responsible for both actin-binding and

bundling. Using this model, regions of the SD1 from mouse and human Shroom2 and Shroom3, containing different conserved elements, were expressed and purified from *E. coli*. The various SD1 proteins were used in the studies described in Chapter 2 to determine the function of each patch and significantly narrow down the sequences in the SD1 that mediate the actin-binding properties of Shroom proteins.

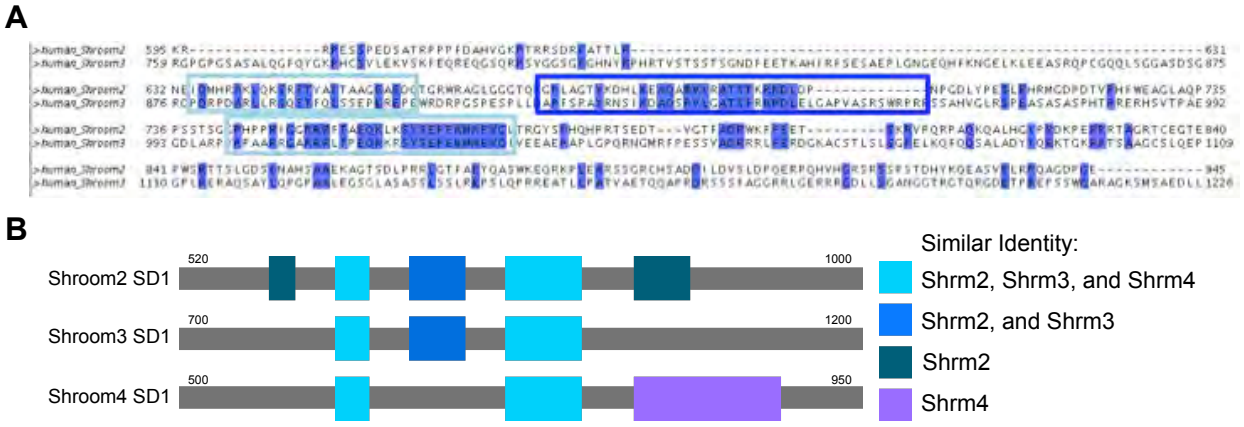

Figure 1.7: Conserved sequence motifs in the SD1s of Shroom2, Shroom3 and Shroom 4.

A) Alignment of Human Shroom2 and Human Shroom3 SD1 regions (ClustalW and JalView). Three patches of conservation are boxed. B) Schematic representation of conserved patches for Shroom2, 3 and 4. While some regions are found across the whole family (light blue), other regions are only found within Shroom3 and Shroom2 (blue). Individual Shroom proteins have regions that are conserved only in that Shroom family member (teal for Shroom2, purple for Shroom4). Numbers represent approximate range represented of the Human isoform of each Shroom's SD1 region.

1.5 GOALS OF THIS RESEARCH

The aim of this research is to define the molecular basis for the Shroom-actin interaction and understand how this interaction influences actin architecture. Toward this end, we will use an entirely *in vitro* biochemical system including binding assays and electron microscopy, which will allow me to directly assess Shroom's role in modifying actin dynamics. Finally, by using both Shroom2 and Shroom3 I can compare each of their SD1's to identify a minimal conserved actin-binding domain.

2.0 SHROOM2 AND SHROOM3 ALTER ACTIN'S ARCHITECTURE WITH THE CONSERVED DOMAIN, SHROOM DOMAIN 1 (SD1)

2.1 INTRODUCTION

All Shroom proteins are characterized as actin-binding proteins. Previous work has shown that the actin-binding module of Shroom2 and Shroom3 are centered around the SD1 [55, 57, 62, 67, 69]. Sequence analysis of this domain across the family reveals a patchwork of conserved amino acids. Evolutionary pressure has presumably led to the maintenance of these conserved patches. However, previous research has yet to determine how the Shroom family is able to mediate an interaction with actin. These patches provide a promising starting point for elucidating the minimal region of the SD1 required for actin binding. I have used proteins of the SD1 from human and mouse Shroom2 and Shroom3 that cover the various patches in an effort to determine a minimal functional region for actin binding.

As mentioned earlier, previous work from our lab has shown that Shroom3 is able to modify actin's architecture [68]. It is not known if Shroom2 or other members of the Shroom family also have this ability. Additionally, the exact nature of how Shroom3 binding alters the organization of F-actin is not known. To this end I have employed transmission electron microscopy to begin to understand what Shroom's SD1 is doing to actin at a structural level. The

goals of this work are to 1) define a minimal region for actin binding and bundling, and 2) define the nature of the actin bundles induced by the SD1 at a structural level.

2.2 RESULTS

2.2.1 Purification of Shroom2 and Shroom3 SD1 proteins

To date, the minimal domain of the SD1 has not been determined biochemically. To further analyze the Shroom family's ability to bind actin and change the architecture of actin filaments, as our previous data suggests [68], I expressed and purified a variety of SD1 protein deletion constructs from mouse Shroom2, human Shroom2, and mouse Shroom3. These proteins covered different portions of the predicted SD1 (Fig. 2.1) with various tags to assist in purification. All constructs contained 6x or 10x His tags and a TEV cleavage site for tag removal. The constructs designed from human Shroom2 also contained a fluorescent Ruby tag that could also be removed with TEV protease. Finally the human Shroom2 constructs also contained C-terminal Arginine hooks. Details about the constructs used can be found in the Materials and Methods, sections 4.1, Table 1. These initial proteins will allow us to begin to determine the minimal SD1 based on conserved patches.

I transformed the corresponding expression plasmids into *E. coli* RIPL cells and induced expression using the auto-induction method [91]. Shrm2A_E, Shrm2B_E, Shrm3BCD, and Shrm3CD were poorly expressed relative to other Shroom domains (Fig. 2.2 & 2.4). In contrast, the Ruby-Shrm2A_D and Ruby-Shrm2CD proteins were expressed robustly (Fig. 2.3) and the Ruby tag appeared to help with solubility. This may prove useful in the design of future SD1

expression plasmids. All of the SD1 proteins exhibit significant degradation (Fig. 2.2, 2.3, and 2.4 elution lanes), however all SD1s were more stable when lysed in pH 8 buffer. Shrm3BCD degraded significantly more than Shrm3CD (Fig. 2.4A vs. B elution lanes). Generally, the shorter proteins (Shrm2B_E, Shrm2CD, and Shrm3CD) were more stable than the longer SD1 proteins (Shrm2A_E and Shrm3BCD). The increased degradation of the larger proteins and increased stability of the smaller proteins supports the hypothesis that there is a stable domain contained within the purified proteins.

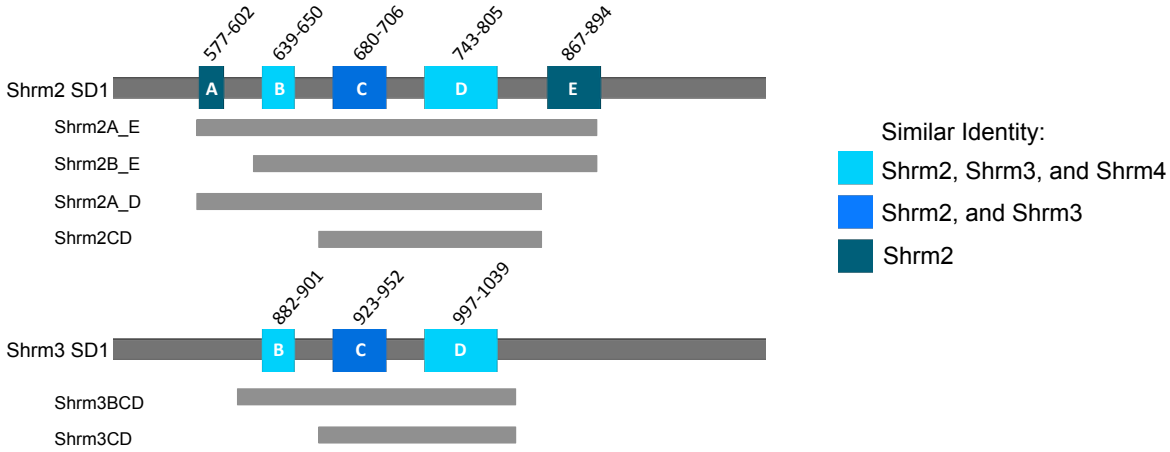

Figure 2.1: The SD1 proteins used in this work.

These proteins were designed and cloned by Ryan Corbo (Shrm2A_D & Shrm2CD) and Ryan Rizaldy (Shrm3BCD, Shrm3CD, Shrm2A_E, & Shrm2B_E). Shrm2A_D & Shrm2CD are derived from human Shrm2 and the Shrm3BCD, Shrm3CD, Shrm2A_E, & Shrm2B_E are from mouse Shrm3 and Shrm2. All proteins contain a 6x or 10x Histidine tag for purification. The Shrm2A_D and Shrm2CD proteins also contain a fluorescent Ruby tag at the N-terminus and an arginine hook at the C-terminus. His and Ruby tags can be removed by TEV cleavage.

All of the proteins could be purified with similar conditions laid out in the materials and methods section 4.2. Shrm2A_E had two prominent degradation products (Fig. 2.2A) that co-purified and contributed to subsequent biochemical assays (Fig. 2.8A). This suggests there may

be a stably folded domain in the purified proteins. Shrm2B_E initially degraded very quickly during purification, however this was rectified by adjusting the lysis buffer to pH 8 (data not shown). Shrm2CD was sufficiently pure after a single Ni-column to be used for further assays (Fig. 2.3). Ni-column flow through, washes, and elution fractions for each purification of an SD1 were run on 12% SDS-PAGE. The gels were then assayed with Coomassie stain to visualize total protein present.

Once the tags were removed, the proteins were run through an additional Ni-column purification. Following Ni-column chromatography, all of the SD1 proteins were diluted into a low salt buffer for cation-exchange chromatography. Elution fractions were analyzed by SDS-PAGE and Coomassie staining for total protein (Fig. 2.2, 2.3, & 2.4 cation-exchange gels). Shrm2A_D eluted later than most of the degradation products when eluted with a sufficiently shallow gradient of NaCl (Fig. 2.3A, cation-exchange). This could be explained if the degradation products lack the arginine hook. The degradation products eluted around 200mM NaCl, similar to that of the other SD1 proteins that did not contain an arginine hook, helping to support this hypothesis.

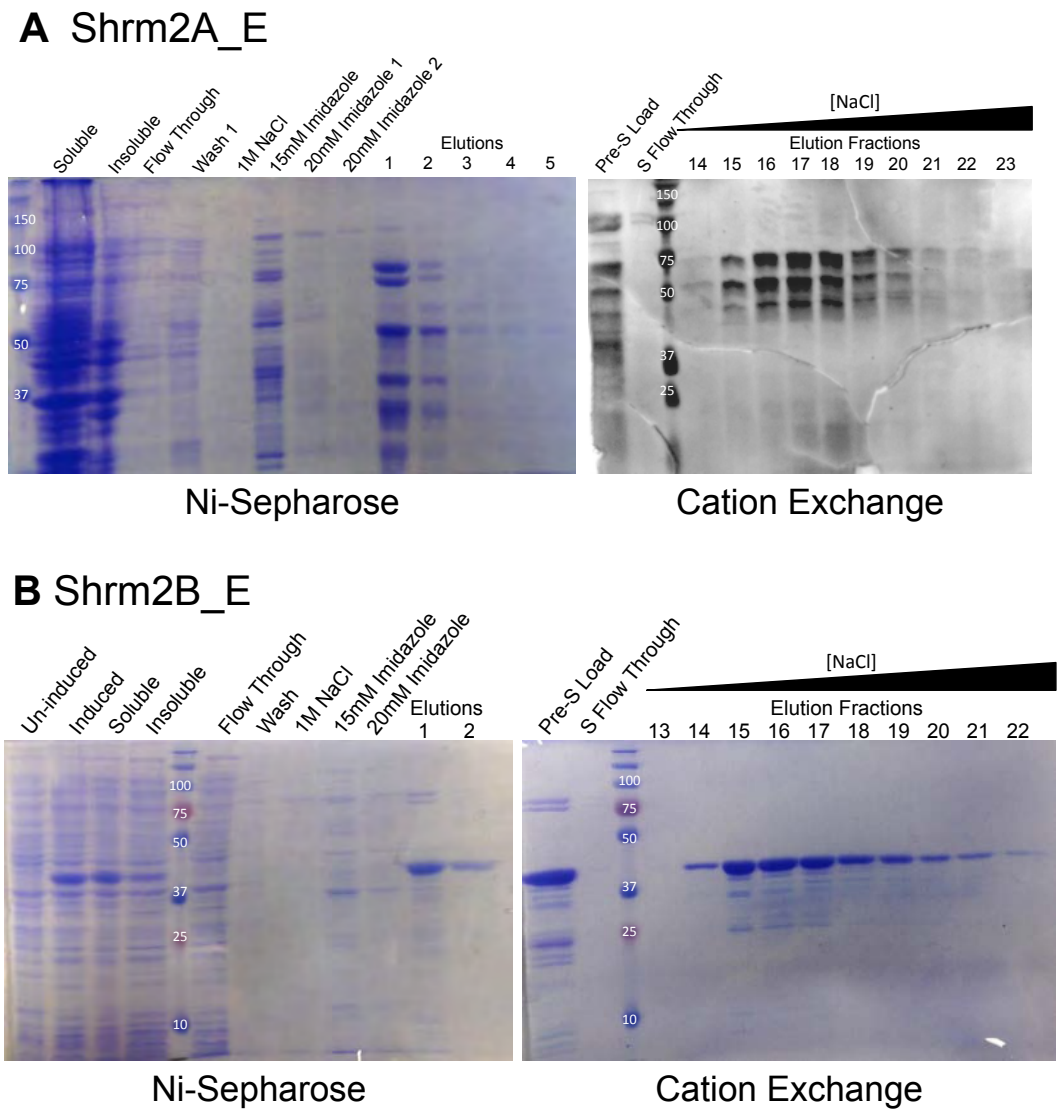

Figure 2.2: Purification of Shrm2A_E and Shrm2B_E.

E. coli were harvested by centrifugation, resuspended in lysis buffer and lysed by homogenization. Cleared supernatant was bound to Ni-sepharose, washed and bound proteins eluted with imidazole. Proteins were further purified with cation-exchange chromatography. A) Ni chromatography and cation-exchange chromatography of Shrm2A_E. Fractions 15-19 were collected and concentrated for use in actin binding and bundling assays. B) Ni chromatography and cation-exchange chromatography of Shrm2B_E. Fractions 15-18 were collected for further assays. Samples were run on 12% SDS-PAGE for 55 mins at 200V and total protein was visualized with Coomassie stain.

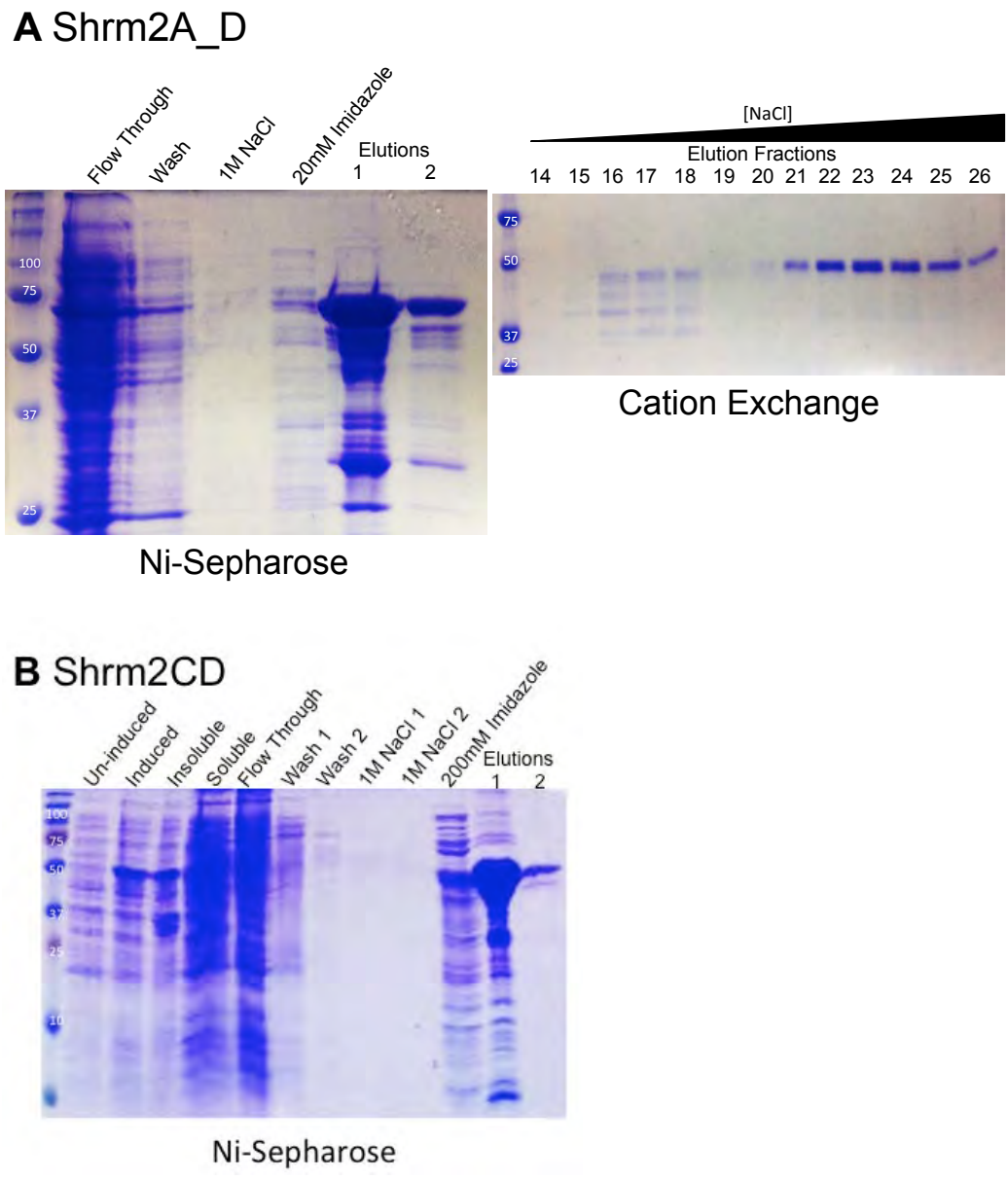

Figure 2.3: Purification of Shrm2A_D and Shrm2CD.

Bacteria were harvested by centrifugation, resuspended in lysis buffer and lysed by homogenization. Cleared supernatant was bound to Ni-sepharose, washed and bound proteins eluted with imidazole. Proteins were further purified with cation-exchange chromatography. A) Shrm2A_D Ni-column chromatography and Cation-exchange chromatography following TEV digest (to remove the Ruby and His tags) and second Ni-column chromatography. Fractions 21-26 were collected and concentrated for F-actin bundling experiments. B) Ni chromatography of Shrm2CD. Samples were run on 12% SDS-PAGE for 55 mins at 200V and total protein was visualized with Coomassie stain.

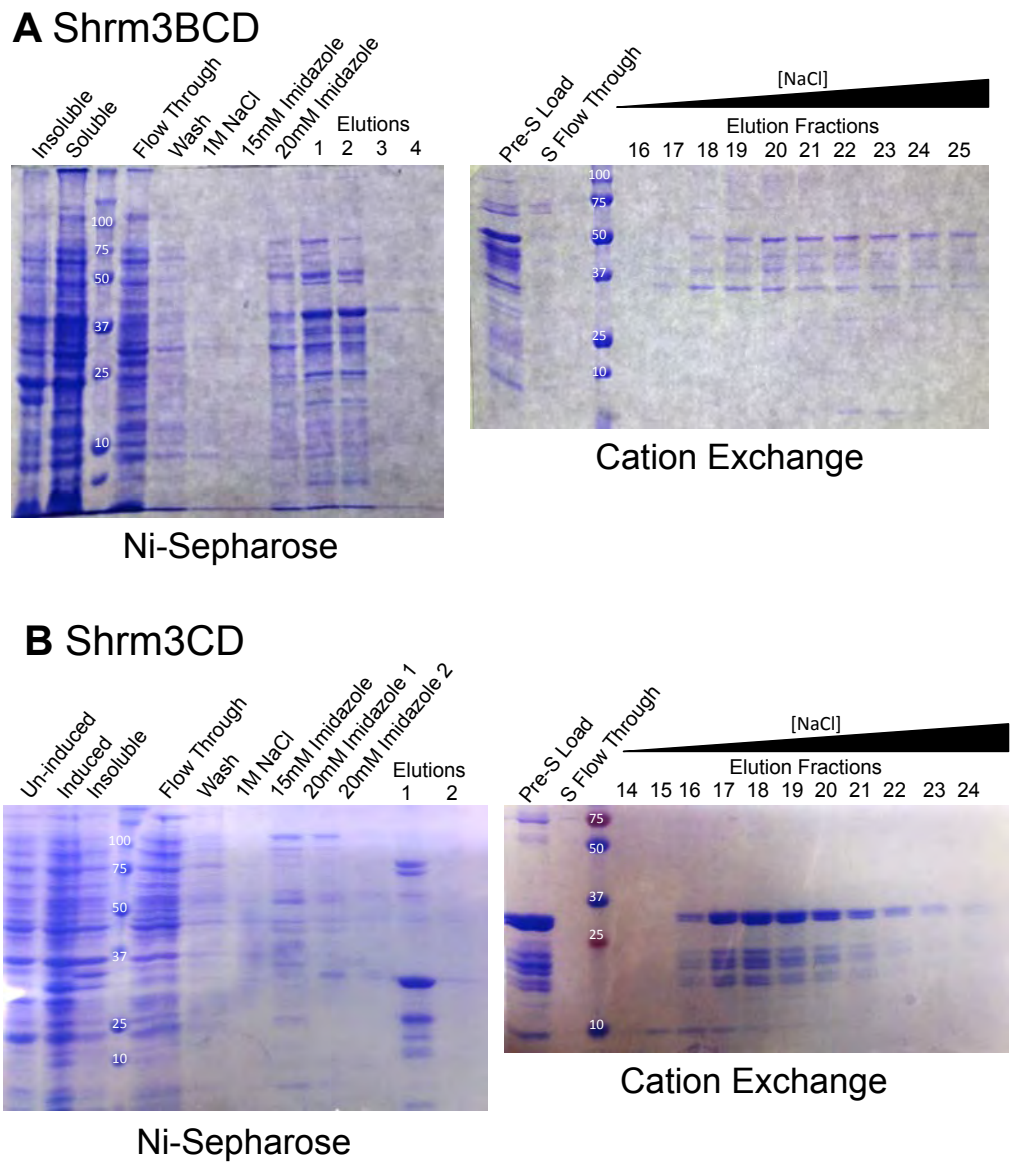

Figure 2.4: Purification of Shrm3BCD and Shrm3CD.

E. coli were harvested by centrifugation, resuspended in lysis buffer and lysed by homogenization. Cleared supernatant was bound to Ni-sepharose, washed and bound proteins eluted with imidazole. Proteins were further purified with cation-exchange chromatography. A) Ni-column purification of Shrm3BCD of lysed cells, B) Cation exchange column of Shrm3BCD. Fractions 19-23 from the Cation-exchange column were for further experiments C) Ni-column purification of Shrm3CD from cells lysed by homogenization. D) Cation-exchange column of Shrm3CD. Fractions 17-20 were collected. Samples were run on 12% SDS-PAGE for 55 mins at 200V and total protein was visualized with Coomassie stain.

After cation-exchange chromatography, the rest of the SD1s were sufficiently pure of contaminants to be used in actin-binding assays. Ruby-Shrm2 (Shrm2A_D and Shrm2CD) proteins were either used for assays immediately following the 1st Ni column, or the Ruby and His tags were removed with TEV proteolysis. While it is possible to concentrate the various SD1s proteins using centrifugal concentrators, I found that a large portion of protein was lost during the process. It is possible that aggregated SD1 bound to the membrane of the concentrators and was not recovered. I predict that the SD1 is susceptible to aggregation or precipitation if buffers are changed drastically and I found that they all have a propensity to degrade (Fig. 2.2, 2.3, and 2.4). Therefore, if possible, elution fractions from the cation-exchange columns were used directly for binding and microscopy studies.

2.2.2 Minimal domain of SD1 still capable of binding actin

Previous work from our lab examined Shroom/actin interactions using a co-sedimentation assay [68, 69]. As an example, I repeated this experiment with a minimal SD1 protein that had not been used in the previous study, Shrm3CD (Fig. 2.1). This protein contains only two conserved patches, but these patches are common to all of the SD1 proteins tested. Purified Shrm3CD was incubated with F-actin at room temperature for 30 minutes and the samples were then centrifuged at 160,000xg. This speed pellets all F-actin and, subsequently, any actin-binding protein present in the sample [92, 93]. When Shrm3CD is pelleted in the absence of actin, approximately 60% of it is found in the pellet. However, in the presence of F-actin, all of Shrm3CD is found in the pellet (Fig. 2.5). This supports our previous data that the SD1 is the actin-binding domain of Shrm. As Shrm3CD is the smallest SD1 construct I tested, these results reduce the boundaries of the actin-binding domain to amino acids 900-1100.

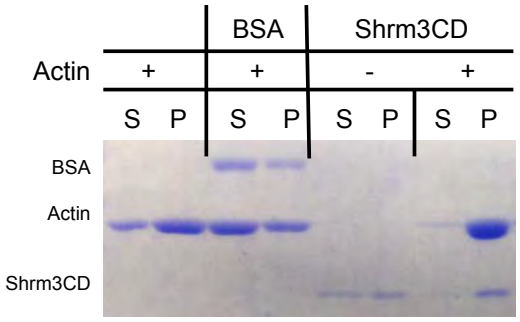

Figure 2.5: A minimal SD1 binds to actin.

Shrm3CD co-sediments with F-actin when the reactions are pelleted at 160,000xg. It also increases the ratio of actin in the pellet compared to actin alone.

2.2.3 Shroom2 and Shroom3 SD1s localize to actin bundles

As an additional test of Shroom/actin interactions, I used confocal microscopy to show that the SD1 proteins not only co-sediment with actin, but also co-localize with actin. I used the same binding reactions as used for the co-sedimentation assay with Shrm3CD, Shrm3BCD and Ruby-Shrm2CD. The Shroom-actin reactions were stained with Phalloidin (F-actin) or α-Shroom3 antibody, spotted on slides, and imaged by confocal microscopy (see Materials and Methods Section 4.4). For Shroom2-actin complexes, Shrm2CD was detected using the Ruby tag. F-actin alone (Fig. 2.6C) or in the presence of BSA (negative protein control, Fig. 2.6A) remains as single filaments and small aggregates. However, when mixed with either Shroom2 or Shroom3's SD1, F-actin aggregates and bundles. These bundles co-stain for Shroom (Fig. 2.6 B", D" & E"). This suggests that Shroom is not only binding actin, but also modifying actin's architecture.

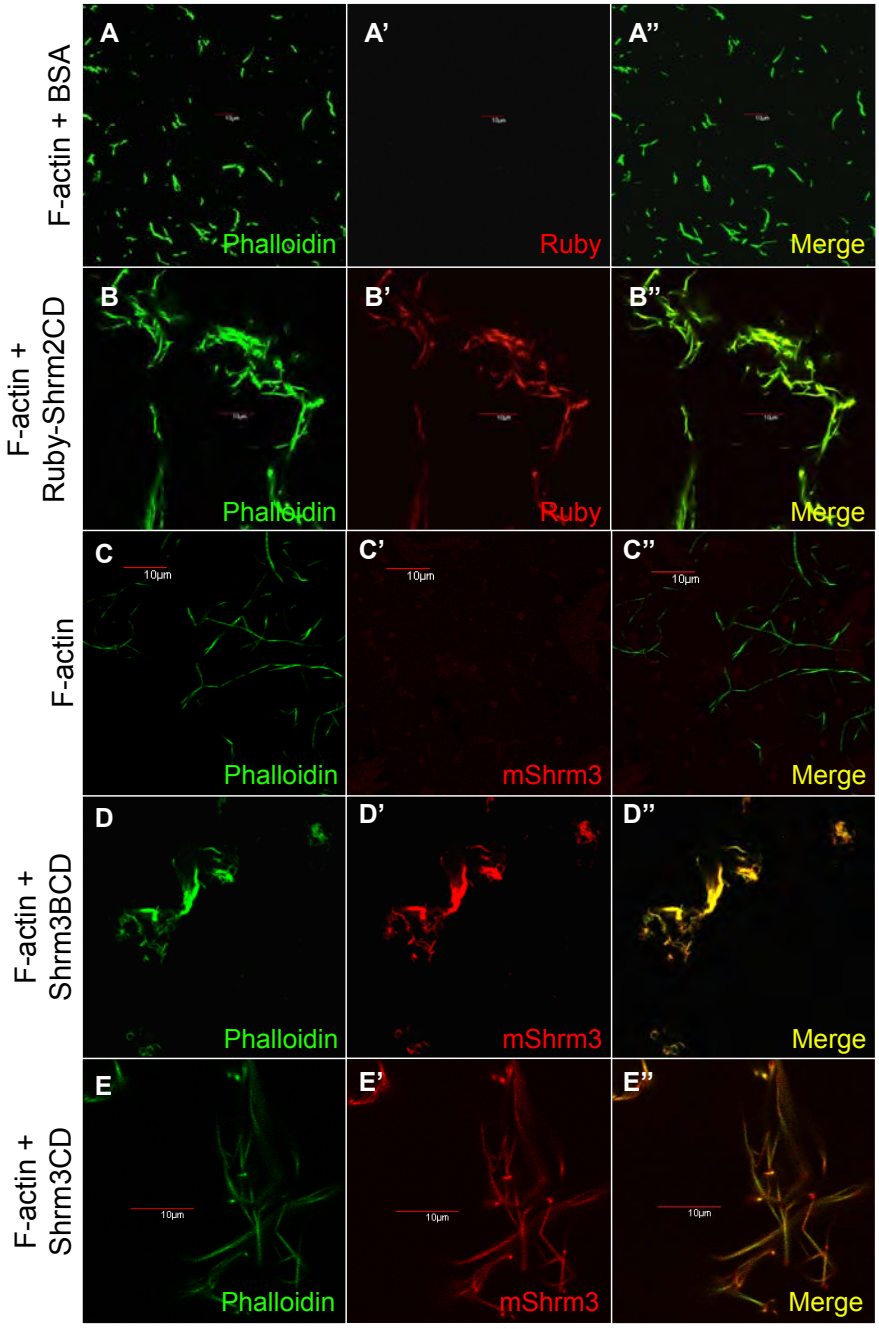

Figure 2.6: Shroom SD1 localizes to F-actin bundles.

A-A'') F-actin with BSA, B-B'') 5µM F-actin plus 5µM Ruby-Shrm2CD. F-actin bundles in the presence of Shrm2CD, C-C'') F-actin, D-D'') F-actin plus Shrm3BCD, E-E'') F-actin + Shrm3CD, A-E: Phalloidin Alexa-488 (1:1000), A' & B': Ruby-tag fluorescence, C'-E': αShroom3, A"-E": Merge

2.2.4 Shroom2 and Shroom3 SD1 induce actin bundles at similar concentrations

My previous experiments using confocal microscopy suggested the SD1 functions to bind and bundle actin. All Shroom proteins are actin-binding proteins, and it appears that Shroom may play a role in changing actin's organization both *in vitro* and *in vivo* [68]. My work has mainly focused on investigating Shroom2 and Shroom3 SD1s' ability to bundle actin *in vitro*. This work will begin to draw a biochemical and structural picture of how Shroom acts as an actin-binding protein. To assess the capacity of the various SD1 proteins that I purified to bundle actin, I utilized a simple assay that relies on differential sedimentation of actin filaments verses actin bundles. When a solution of F-actin is centrifuged at 14,000xg only bundled F-actin will pellet, whereas G-actin and single filaments will remain in the supernatant [93]. These assays will also co-sediment proteins that are bound to the actin bundles. An increase in the amount of bundled actin in the pellet when SD1 is added would suggest that the SD1 is responsible for actin bundling by Shroom.

Initially all proteins were tested with Shroom in excess to determine the absolute ability of each protein to bundle F-actin. All SD1 proteins I worked with were capable of bundling actin. For example when mixed with Shroom3 SD1 (Shrm3BCD or Shrm3CD), approximately 80% of the F-actin pellets following low-speed centrifugation (Fig. 2.7).

Repeating this experiment with the additional SD1 proteins from Shroom2 and Shroom3 induced bundling of approximately 50% of the actin present with μM affinity (50% of 5uM of F-actin was bundled by 0.5μM to 1μM Shroom SD1) (Fig. 2.8). This ratio held true even for the smallest SD1 proteins for both Shroom2 and Shroom3 (Shrm2CD and Shrm3CD) (Fig. 2.8 D and E). The exact ratios of bundled to unbundled actin had a degree of variability (Fig. 2.8, % of F-actin in the pellet).

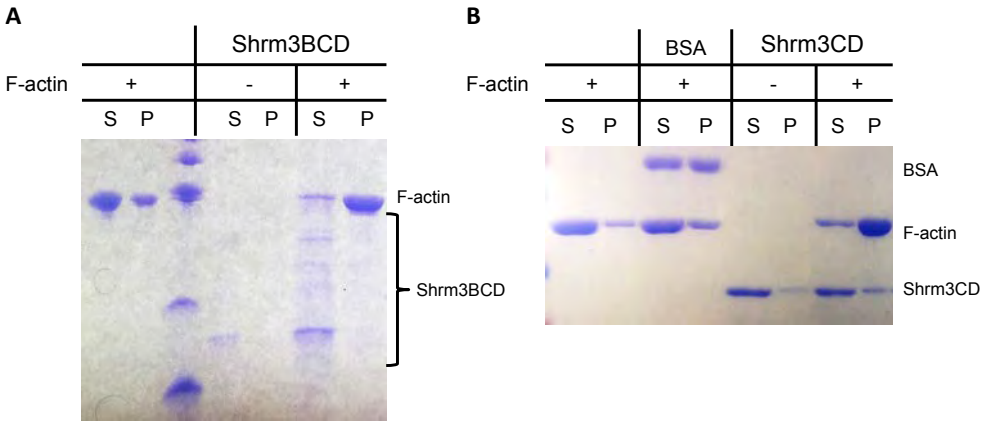

Figure 2.7: Shroom3 SD1 bundles F-actin.

Addition of Shrm3BCD (A) or Shrm3CD (B) induces bundling of actin *in vitro*. Shrm3CD is more stable than Shrm3BCD, which degrades. This could suggest that Shrm3CD represents the stable domain. Reactions were run on 12% SDS-PAGE for 50 minutes at 200V and total protein was visualized with Coomassie stain.

The actin binding reactions were also run for varying lengths of time in addition to varying the concentrations of SD1 then. I found that within 10 minutes, 1µM Shroom SD1 was sufficient to bundle F-actin to a similar degree as the 30-minute standard reaction. When Shroom is in excess, the shortest time point (less than 1 minute) was sufficient to bundle F-actin to the same level as the standard 30-minute reaction (data not shown).

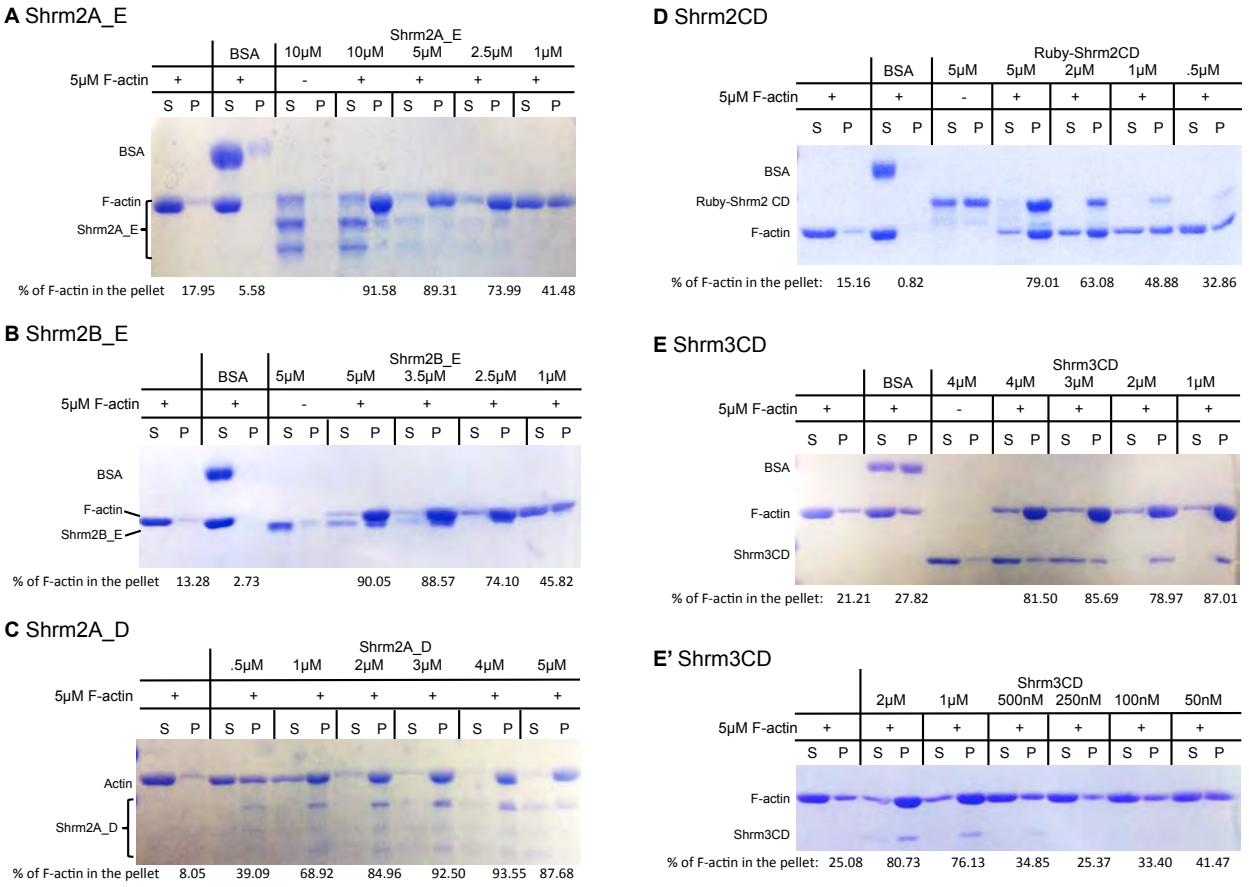

Figure 2.8: Shroom2 and Shroom3 induce bundling of F-actin with nM affinity.

Varying concentration of the indicated Shroom2 or Shroom3 SD1 proteins were added to a fixed amount of F-actin, incubated for 30 minutes at room temperature and centrifuged for 1hr at room temperature at 14,000xg. A) Shrm2A_E, B) Shrm2B_E, C) Shrm2A_D, D) Shrm2CD, E) Shrm3CD 1uM to 4uM, E') Shrm3CD 50nM to 2uM.

2.2.5 Shroom2 and Shroom3 SD1s induce the formation actin bundles with similar architecture.

I established that all of the tested SD1 proteins are capable of inducing actin bundling (Fig. 2.7 and 2.8). However, since the bundling assay only assesses the formation of large structures, it was not known if these proteins induce the formation of bundles with the same architecture or

organization. Given that these two family members localize to different actin populations, with different architectures, it is possible that the SD1s of Shroom2 and Shroom3 order the actin fibers differently.

Historically, EM has been a common method for visualizing actin as well as actin-binding proteins at nm resolution [12, 15, 46, 94-96]. The ability to visualize individual filaments removes the need for molecules to pack in a regular lattice as required by x-ray crystallography. Additionally, F-actin filaments themselves are not always ordered the same way within a bundle and thus would not be uniform enough to achieve ordered diffraction. Another thing to consider when dealing with the bundling of actin is that one bundle may not, and likely variability will not be, exactly the same as another bundle. Differences in the number of F-actin filaments forming the bundle, and uneven distribution of the actin-binding protein both contribute to the difficulty in understanding these complex structures at an atomic scale. To date there are no published 3D reconstructions of an actin bundle formed *in vitro*. Current models are based on structures of single F-actin filaments bound by actin-binding proteins [97-99]. However, to achieve these structures, either actin or the actin-binding proteins had to be modified so as not to form actin bundles [46, 96]. To accomplish my goals, I first had to understand qualitatively the architecture of the SD1-induced F-actin bundles. I used this information to formulate hypotheses about how the SD1 induces the formation of the F-actin bundles.

Toward this end, I used Transmission Electron Microscopy (TEM) to further analyze the structure of the F-actin bundles formed in the presence of the Shroom SD1s. To generate samples for TEM analysis, actin bundles were generated as described in the previous section, however samples were immediately spotted on grids and negative stained. Using a floating carbon method

to make the grids, developed by Dr. Duda (see Materials and Methods), greatly reduced the background noise as compared to those grids that were pre-coated in carbon.

The SD1 proteins of Shroom2 and Shroom3 induce bundles (Fig. 2.9). The SD1 proteins from Shroom2 and Shroom3 induce the formation of actin bundles that have roughly the general appearance of parallel or anti-parallel bundles of highly-packed filaments, ranging from a few filaments (15nm in width) to many filaments (~100nm in width) (Fig. 2.9). For example, Shrm2A_D, one of the longest SD1 proteins containing all of the core elements, induced the formation of bundles with an architecture similar to those induced by Shrm3CD, one of the shortest, most minimal SD1 proteins (Fig. 2.9D and 2.9G) This observed similarity suggests that conserved patches C and D may constitute the minimal SD1 and confer Shroom's ability to bind and bundle actin. The high level of variability between bundles, even within the same sample, can likely be attributed to the fact that forming bundles is a dynamic process and with EM we are able to see every stage of bundle formation. We can see bundles that may represent the early stages of actin-bundling consisting of only a few filaments (Fig. 2.9E), to the more organized, larger, possibly later stages of bundling (Fig. 2.9G).

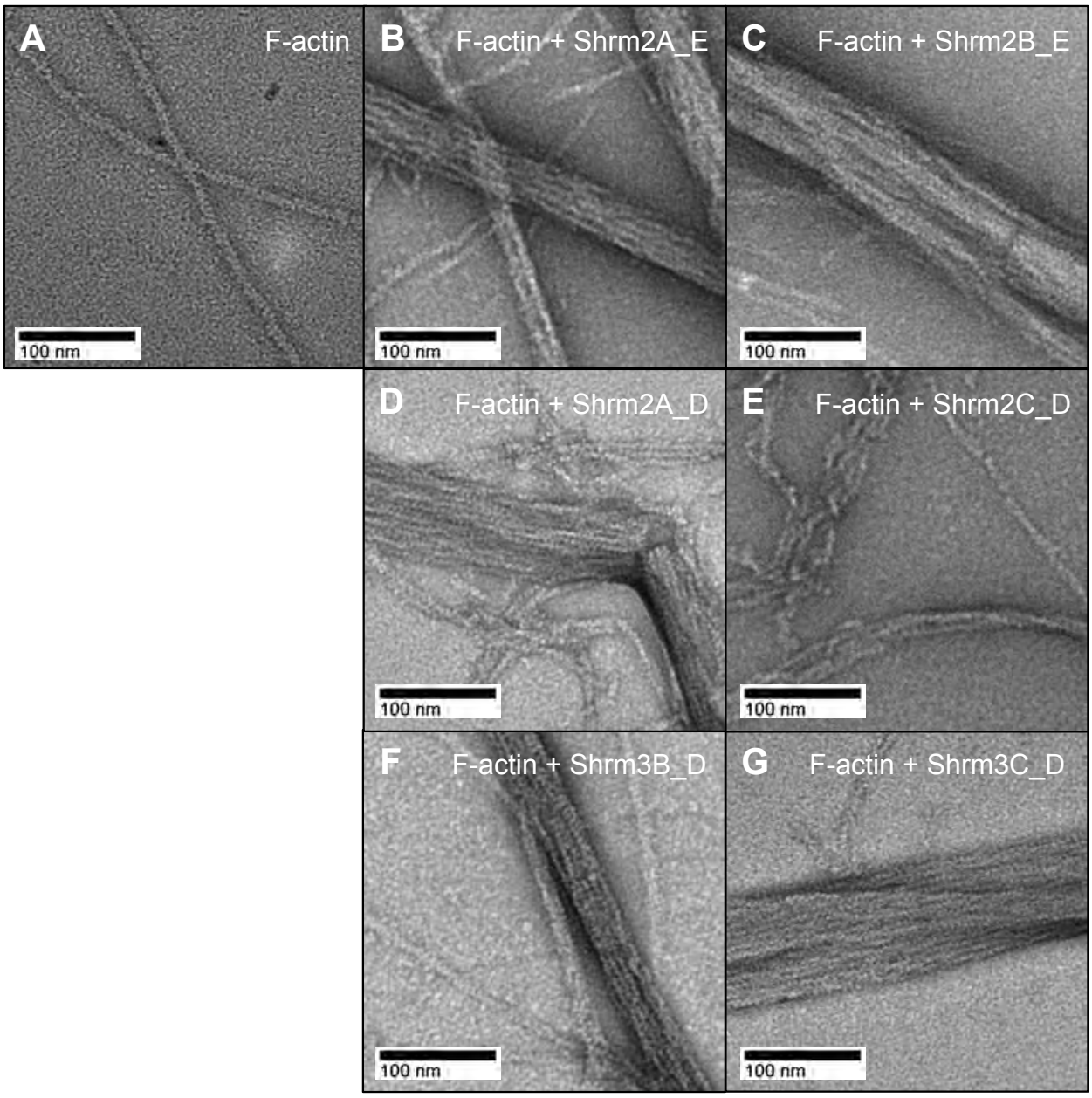

Figure 2.9: Shroom induced actin bundle formation.

F-actin or F-actin plus the indicated SD1 proteins were mixed at room temperature for 30 minutes, spotted on grids, and observed via TEM. All SD1 proteins tested induced the formation of bundles with a range of diameters. A) F-actin alone, B) F-actin with Shrm2A_E, C) F-actin with Shrm2B_E, D) F-actin with Shrm2A_D, E) F-actin with Shrm2CD, F) F-actin with Shrm3BCD, G) F-actin with Shrm3CD.

To more precisely define bundling structure, we analyzed several of our micrographs. For example, Shrm2A_E induced a small bundle of actin that had a very regular pattern (Fig. 2.10) that forms a repetition between a narrow region and a wider region. To analyze these bundles further I utilized Fast Fourier Transforms (FFT) to enhance the images (see Materials and Methods 4.6 and Appendix B). When looking at the inverse FFT, we can see that this structure is likely composed of two F-actin filaments next to each other. The bulbous point that we see in the original image likely reflects the cross over point of F-actin: the spacing of these points is approximately 365Å, as is more apparent in the inverse FFT, which correlates with the known cross over spacing for an F-actin filament (360Å). The distance between filaments is approximately 5nm. Repeated attempts to replicate the exact same bundle shape produced a range of actin bundle sizes, some very similar to that seen in 2.10A. It is possible this small bundle, which likely consists of only 2 actin filaments, based on the total width measurement of each filament (6.5nm) and the inverse FFT (Fig. 2.10B), is a precursor bundle to some of the larger bundles we also observe. Because of its highly ordered structure we have also pursued Cryo-EM of the actin bundles formed by this SD1. We have successfully frozen grids that contain the actin bundles of various sizes (Fig. 2.10C). Our collaboration with the Conway lab in the Department of Structural Biology will hopefully lead to a 3D reconstruction of the actin bundle formed *in vitro*.

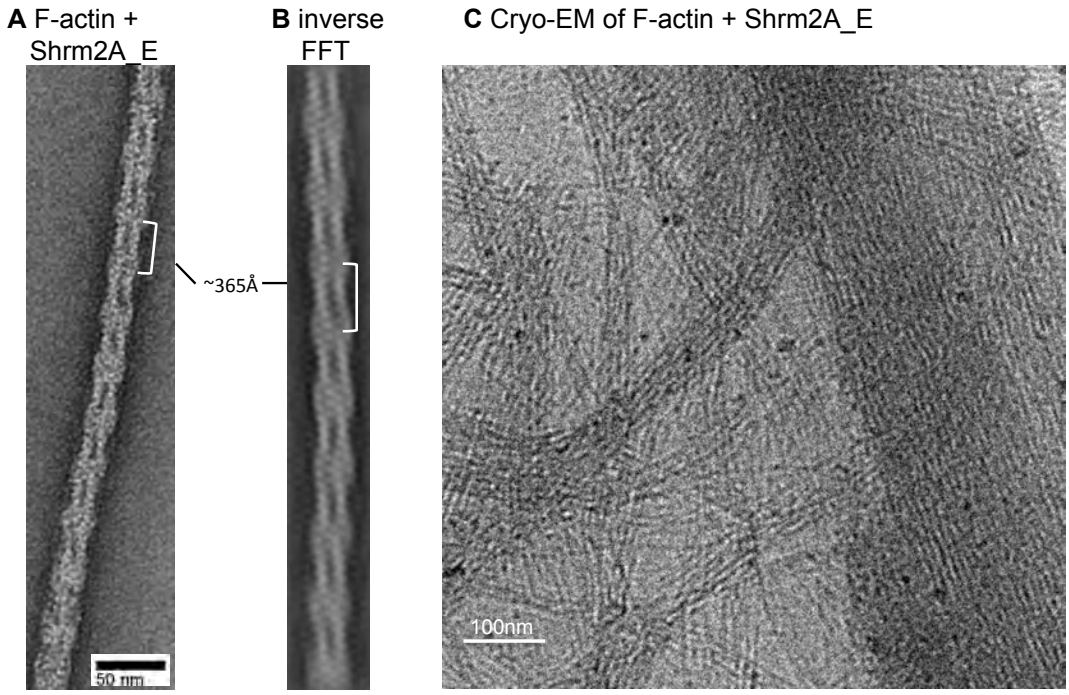

Figure 2.10: Shrm2A_E induced actin bundles.

A) Ordered F-actin bundle of F-actin with Shrm2A_E, B) The inverse FFT shows that the right bundle is likely made up of 2 parallel F-actin filaments, C) TEM of preliminary Cryo-EM grid with F-actin bundles induced by Shrm2A_E. We can see a wide range of sizes of bundles and the filaments of actin look well ordered.

Closer examination of a bundle formed by Shrm2B_E, a protein that encompasses almost the entirety of the predicted Shroom2 SD1, and a bundle of the same size formed by the most minimal region of the Shroom3 SD1, Shrm3CD, reveal several similarities (Fig. 2.11). If we preform a Fast Fourier Transform (FFT) on a segment of the bundle, and trim the data to remove artifacts from the microscope, we can calculate an inverse FFT of this data (see appendix B). As we can see in Fig. 2.11, comparing A' and B' indicated strong similarity to the spacing of the F-actin filaments. Also, the filaments are packed in parallel or anti-parallel bundles.

Taken together, these data suggest several interesting properties of the SD1. First, they suggest that the minimal functional SD1, at least for actin bundling, consists of the conserved

core elements C and D. Second it suggests that the actin bundles induced by the SD1 consist of parallel or anti-parallel bundles, as opposed to a mesh or some other higher order network. Third, it suggests that the other conserved sequence elements may be involved in other aspects, such as regulation.

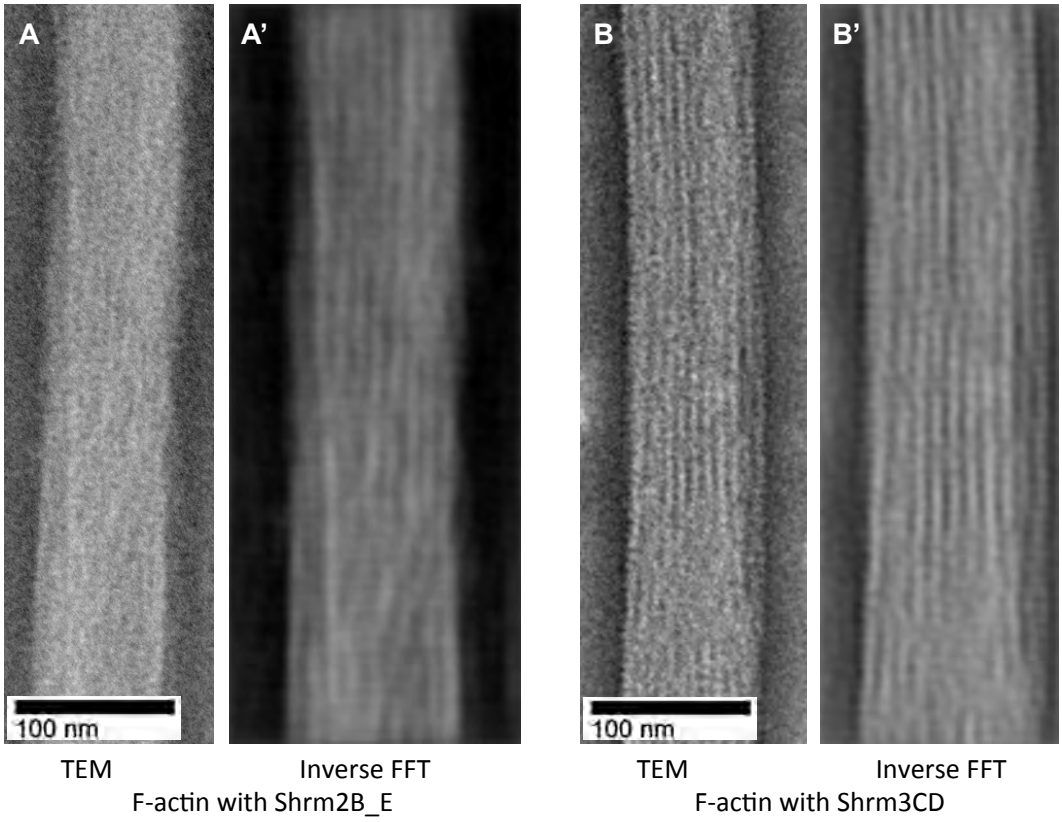

Figure 2.11 Shroom2 and Shroom3 induce the formation of actin bundles with similar architecture.

A) TEM of a F-actin bundle induced by Shrm2B_E. A') Inverse FFT of this bundle. We can see the separation of the F-actin filaments more clearly once the data has been trimmed. B) TEM of a F-actin bundle induced by Shrm3CD B') Inverse FFT of the bundle. Given that the starting image was more in focus, it contained more data. This increase in data allows more information to be apparent in the inverse FFT. The light lines are the F-actin filaments, the dark gaps are the spaces between filaments.

3.0 DISCUSSION AND FUTURE DIRECTIONS

3.1 ACTIN BUNDLING IS CONSERVED BETWEEN SHROOM2 AND SHROOM3

We show here that Shroom is a potent actin bundling protein, capable of bundling actin in lower concentration ratios than that of Villin, an actin-binding that protein that forms bundles of similar architecture. For comparison, Villin reached maximal bundling at a ratio of 1.5μM Villin to 3μM F-actin [41]. The Shroom SD1s I tested reached maximal bundling at around 1.5μM SD1 to 5μM F-actin. Shroom SD1s were able to induce bundling of 50% of the F-actin at molar ratios as low as 250nM SD1 to 5μM F-actin. This ratio could help us to hypothesize about occupancy of Shroom along F-actin filaments and bundles. It is possible that Shroom is more dispersed across the bundle than has been predicted and modeled for Villin and Fimbrin [23, 41, 97].

In comparing Shroom's actin bundles to those formed by Villin and Fimbrin, we see similar spacing of filaments, around 4.5-5nm [24, 25, 97]. This small spacing helps us to understand how Shroom bundles actin. We can rule out a scenario such as that of α-Actinin which dimerizes in such a manner to space the filaments approximately 30nm apart [26]. While the spacing between filaments is similar in Shroom-induced bundles and Villin- or Fimbrin-induced actin bundles, there are differences. As discussed above, Shroom reaches maximal bundling of actin at a lower molar ratio than that of Villin. I was able to induce the formation of ordered bundles of actin up to 100nm in diameter. There is some evidence that Villin is also

capable of forming large bundles *in vitro*, supporting the biological relevance of bundles of this size. Villin and Fimbrin provide us two possibilities for how Shroom is able to bundle actin. The SD1 either forms a dimer that positions the two actin-binding motifs in close proximity (similar to Villin), or it contains two actin-binding motifs in close proximity (Fimbrin).

Taken together, we conclude that Shroom likely plays a powerful role in regulating actin's architecture during morphogenesis. For the anisotropic changes to cell shape to be achieved it would be beneficial for Shroom to easily induce the formation of actin bundles while also recruiting Rock to the actomyosin network. This bundling of actin by Shroom could also play into the regulation of Rock by Shroom and the subsequent regulation of myosin activity on the actin bundles themselves. Through bundling actin, Shroom levels could be increased in localized areas, leading to localized upregulation of Rock. As our research continues, it appears that this pathway feeds back on itself with multiple levels of regulation affecting multiple aspects. On one level, Shroom acts a scaffold between actin and Rock as well as other upstream proteins, like Dishevelled [2]. On another level, Shroom regulates the activity of Rock as well as the architecture of actin. Shroom appears to play a complex role in regulating changes to cell morphology.

3.2 FUTURE DIRECTIONS

The next steps of this project will be to define the actin-binding and/or dimerization motif(s) located within the minimal region of the SD1. There are a variety of actin-binding proteins, as well as the myriad of actin-binding motifs [22, 27, 100]. Many of these actin-binding proteins or protein families contain a unique actin-binding motif. This seems to be the case for Shroom as

well. Now that I have determined a minimal actin-binding/bundling region, we can investigate important residues for these activities. With this smaller region, we should focus on the most well-conserved amino acids of the two patches. Once an actin-binding motif is found, we can look in the Shroom family members that have been less well studied, and search for the same motif. We can use the fact that there is little conservation across the whole family to look for invariant residues as possible targets.

With this work we are left with 2 possible models for how Shroom is able to both bind and bundle actin. Shroom either contains a single actin-binding motif, then dimerizes in an orientation that spaces the sites around 4.5 nm apart, or Shroom contains two actin-binding sites. To this end, mutational analysis of single patches could reveal highly informative separation of function variants, which can bind but not bundle or still form multimers and not bind actin. It would be interesting to see if each conserved patch were able to bind actin alone, or if each has it's own role and they are not redundant. The oligomeric state of Shroom has been a point of interest for us since our collaborators solved the structure of the dShroom SD2 revealing an anti-parallel dimer [70]. However, the structure of human Shroom2's SD2 bound to Rock's SBD recently solved by Jenna Zalewski suggests that the human Shroom2 SD2 binds Rock as a monomer (unpublished work). This dichotomy leaves the question of Shroom's oligomeric state unresolved. To determine if the SD1 is a monomer or some higher order oligomer, a crosslinking assay could be done.

Finally given the potential of Shroom to induce regular bundles *in vitro*, it provides a promising target for Cryo-EM with the goal being the first 3D reconstruction of an *in vitro* actin bundle. The architecture of the bundles formed by Shroom2 and Shroom3 are so similar that a model could be applied to both family members. This reconstruction would give us a new level

of understanding of what is happening within the cell on a structural level. Cryo-EM has proved to be the method of choice for structures of F-actin and F-actin in complex with ABPs [12, 15, 23, 25, 95, 97]. We have preliminarily made Cryo-grids that contain actin bundles induced by Shroom, suggesting this may be a feasible approach. We hope to use this approach in the future to not only determine Shroom's occupancy of the actin filaments, but also if Shroom is modifying the helical pitch of F-actin. It has been shown in other cryo-EM reconstructions that F-actin can be found with different helical pitches and polymorphisms. Finally, we hope to be able to solve the structure of the SD1 bound to F-actin as well as a 3D reconstruction of an *in vitro* formed actin bundle.

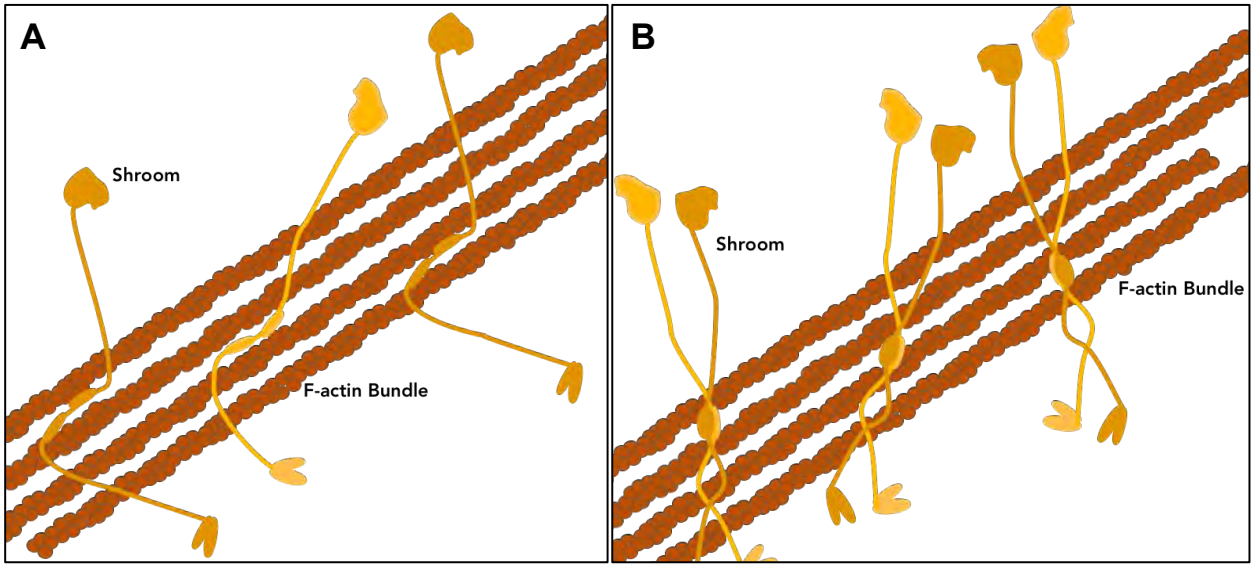

Figure 3.1: Possible models for Shroom's method of bundling actin.

A) Shroom could contain 2 actin-binding motifs and span 2 f-actin filaments. B) Or Shroom could form a dimer and each monomer of Shroom would contain 1 actin-binding motif. The dimer of Shroom would bind multiple F-actin filaments to induce bundling.

4.0 MATERIALS AND METHODS

4.1 PLASMIDS

Table 1: Plasmids used in these studies

Name (previous name)	cDNA source	Amino Acids	Vector	Tags contained	Cleavage site	Cloned by
Shrm2A_E (mShrm2 573-921)	Mouse Shroom2	573-921	pET 151 [101]	N: 6xHis	TEV site after 6xHis	Ryan Rizaldy
Shrm2B_E (mShrm2 626-921)	Mouse Shroom2	626-921	pET 151 [101]	N: 6xHis	TEV site after 6xHis	Ryan Rizaldy
Shrm2A_D (hShrm2 565-843)	Human Shroom2	565-843	*pXH2 10xHis Ruby [102]*	N: 10xHis & Ruby; C: Arginine Hook	TEV site after Ruby	Ryan Corbo
Shrm2CD (hShrm2 669-843)	Human Shroom2	669-843	*pXH2 10xHis Ruby [103]*	N: 10xHis & Ruby; C: Arginine Hook	TEV site after Ruby	Ryan Corbo
Shrm3B_D (mShrm3 750-1100)	Mouse Shroom3	750-1100	pET 151 [101]	N: 6xHis	TEV site after 6xHis	Ryan Rizaldy
Shrm3CD (mShrm3 900-1100)	Mouse Shroom3	900-1100	pET 151 [101]	N: 6xHis	TEV site after 6xHis	Ryan Rizaldy

4.2 PROTEIN PURIFICATION

SD1 proteins of mShrm2, mShrm3 and hShrm2 were purified from RIPL *E. coli* cells. Briefly; DNA was transformed into BL21 RIPL cells and grown overnight at 37C to saturation. Overnight culture were used to inoculate 1-2 L cultures and protein expression achieved via

auto-induction for approximately 24 hrs at RT. Bacteria was pelleted for 10 minutes at 6000xg, flash frozen in liquid nitrogen, and stored at -80°C until lysis. Cells were resuspended in lysis buffer (500mM NaCl, 25mM Tris-Base, 8% Glycerol, 5mM Imidazole, 1mM βME, pH 8) plus a protease inhibitor cocktail. Bacteria were resuspended with a ratio of 10 mg of cells per 1 mL of lysis buffer. Bacteria were lysed via homogenization using an Avestin Emulsiflex homogenizer. Insoluble material was removed via centrifugation for 30 minutes at 12,000xg. The supernatant was run over a Ni^{2+}-column to allow for purification of his-tagged proteins. The column was sequentially washed with Lysis Buffer, Lysis buffer containing 1M NaCl, Lysis Buffer with 15mM Imidazole, and then Lysis Buffer with 20mM Imidazole. His-tagged protein was eluted with either 200mM Imidazole buffer (mShrm2 and mShrm3) or 1M Imidazole buffer (Ruby-hShrm2). The higher concentration of imidazole was necessary to release the 10xHis tag of the Ruby-hShrm2 proteins. Results were analyzed by SDS-PAGE and total protein was visualized with Coomassie stain.

The 6xHis tag was not removed from the mShrm2 and mShrm3 proteins because skipping the TEV cleavage step reduced the degradation of the proteins by shortening the total purification time. The Ruby-hShrm2 proteins were more stable and were able to be treated with his tagged TEV protease to remove the Ruby and His tags. Cleavage reactions were run over a second Ni-column to separate free hShrm2 SD1 from the Ruby tag and TEV. The appropriate fractions from the Ni-columns were diluted into a low salt buffer (final NaCl concentration of 100mM, pH 7.5) and run over a cation-exchange column to purify away contaminating proteins.

Ruby-Shrm2 (Shrm2A_D and Shrm2CD) proteins were either used for assays immediately following the 1st Ni column, or the Ruby and His tags were removed with TEV proteolysis. Once the tags were removed, the proteins were run through an additional Ni-column

purification. The cleaved SD1 proteins flowed through and the un-cleaved fusion protein, the tag, and TEV (which itself has a His tag) remained on the Ni-column. Following Ni-column chromatography, all of the SD1 proteins were diluted into a low salt buffer (100 mM NaCl, 20 mM Tris, 8% Glycerol, 1mM βME, pH 7.5) for cation-exchange chromatography. All proteins would precipitate if left to dialyze into a low salt buffer for too long. For this reason, the salt and pH had to be lowered by dilution instead of dialysis. To further minimize the propensity of the SD1s to precipitate, I increased the glycerol concentration from 2% to 8%, increased the pH from 7 to 7.5, and made the final salt concentration 100mM instead of 50mM. The Shrm2A_D and Shrm2CD proteins also possess an arginine hook, which aids in purification via cation-exchange chromatography even at pH 8. The SD1s were eluted off the cation exchange with a gradient of increasing salt concentration. Shrm2A_E, Shrm2B_E, Shrm3BCD, and Shrm2CD eluted between 200mM and 300mM NaCl, owing to their similar pIs. The Shrm2A_D and Shrm2CD proteins eluted between 350 and 450mM NaCl due to their increased affinity for the cation-exchange because of the arginine hook

4.3 ACTIN

4.3.1 Actin Polymerization

Actin (catalog number: AKL95) was polymerized into F-actin as described by the manufacturer (Cytoskeleton, LLC). Briefly; G-actin lyophilized powder was resuspended in 250µL of General actin Buffer (GAB, 5mM Tris, 0.2mM $CaCl_2$, pH8) to 1mg/mL. Allowed to incubate on ice for

30 minutes. 25µL of 100mM ATP was added to induce polymerization of G-actin into F-actin [92, 93]. Final actin stock concentration 21µM.

4.3.2 Actin Binding Reaction

5uM actin was allowed to react with the purified SD1 proteins at various concentrations in GAB for 30 minutes at room temperature (RT). For control reactions, actin was either left alone or allowed to react with 1µM BSA. The reactions were then used for the following experiments.

4.3.3 Analysis of actin Binding or Bundling via Differential Centrifugation

Analysis of actin binding and bundling was performed as described by manufacturer (Cytoskeleton, LLC). For actin-binding, F-actin was mixed with purified SD1, incubated at RT, and centrifuged at high speed (160,000xg in a Beckman airfuge for 1 hour). At this speed, all the F-actin is pelleted and G-actin remains in the supernatant [92, 93, 104]. The supernatant was removed from the pellet and the pellet was resuspended in an equal volume GAB and 10x SDS Sample buffer added to a final concentration of 1x. Samples were analyzed by SDS-PAGE and total protein was visualized with Coomassie stain.

To assay F-actin bundling, the actin binding reactions were spun at a low speed as described by the manufacturer (Cytoskeleton, LLC) to pellet bundled F-actin and the associated actin bundling proteins. The reactions were centrifuged at 14,000xg for 1hr [104]. The supernatant was removed from the pellet and the pellet was resuspended in an equal volume GAB and 10x SDS Sample buffer added to a final concentration of 1x. Samples were analyzed by SDS-PAGE and total protein was visualized with Coomassie stain.

4.4 CONFOCAL MICROSCOPY OF ACTIN BUNDLES

Shrm3 SD1 proteins were allowed to react with actin, as described above. The reactions were incubated with a mixture of mShrm3 antibody (UPT132, [6]), Alexa568-conjugated secondary antibody (A-11036, Invitrogen), and Alexa Fluor 488 Phalloidin (A-12379, Thermo Fisher) (1μL of each in 10μL total master mix, 1μL of mix per reaction). Additionally due to the inability to wash away unbound antibody, the reactions were diluted 1:1 in mounting medium. This greatly reduced background fluorescence from the secondary antibody. After incubation with the antibodies and Phalloidin, the reactions were mounted on slides, and imaged using a Flowview Olympus Confocal microscope under 40x and 60x oil objectives.

To image the actin bundling ability of Shrm2 SD1, the above reactions were performed using Ruby-Shrm2A_D or CD, described above. Actin was detected using Alexa488 Phalloidin (1:10 dilution, 1μL per reaction). Slides were prepared and imaged in the same manner as above.

4.5 EM GRID PREPARATION

4.5.1 TEM grids

Actin/Shroom bundles were prepared as above and imaged via negative stained EM grids with Transmission Electron Microscopy (TEM) in two ways. The first method was as follows: 400 mesh Copper grids coated in Formvar and Carbon were glow discharged for 1 min. 10 μL of sample was spotted on the grid and incubated for 30 seconds at room temperature. The sample was rinsed 6 times with ddH_2O for a total of 30 seconds. A solution of 1% Uranyl Acetate was

spotted on the grids. The Uranyl Acetate was replaced 2 times, for a total staining time of 30 seconds. Grids were dried with Whatman filter paper and stored at RT. The second method utilized 400 mesh Copper grids with no coating. Mica, sputter coated with Carbon, was trimmed into a thin rectangle. This piece of mica was slowly inserted into a convex drop of approximately 170 µL of actin or actin with Shroom SD1, then ddH_2O, and finally 1% Uranyl Acetate negative stain. This was done at a fixed 45-degree angle, so the carbon would float on the surface, with each step lasting 30 seconds. While the mica was in the negative stain, an uncoated grid was touched to the surface of the drop to pick up the floating carbon. This method provided less coverage of the grid, but reduced background noise with a more even negative stain of the sample. Images where taken on the FEI-Morgagni at the University of Pittsburgh, Department of Biology, SRSS Facility. Briefly, negative stained grids were imaged at 80V with magnification between 7,100x (.006915 µm/pix) up to 140,000x (.318008 nm/pix).

4.5.2 Cryo-Grids

Cryo-Grids were prepared with actin bundling reactions consisting of F-actin and Shrm2A_E. The reactions were run as described above but for 10-20 minutes, instead of 30 minutes to reduce the size of the actin bundle, prior to being spotted on 400um grids coated with carbon. The carbon coating contained evenly spaced holes for the vitreous ice to form, but also allowed the actin bundles to stick to a surface and span the holes. The carbon coating was essential because tests of grids without the carbon coating did not contain any actin bundles. The sample was blotted from one side only for 8 seconds then plunged into liquid ethane and stored in liquid nitrogen. This was done on a FEI-Vitrobot in Dr. Conway's lab at the Department of Structural Biology at the University of Pittsburgh School of Medicine. It was critical to blot from only 1

side, as large objects can be blotted away from the grids when the standard 2-sided blotting it performed. Preliminary images were taken on the FEI-Tecnai F-20 at the Department of Structural Biology, University of Pittsburgh School of Medicine.

4.6 FAST FOURIER TRANSFORM (FFT) AND INVERSE FFT

Image of actin bundles and filaments were first rotated in NIH ImageJ so that the filaments of the bundles ran longitudinally. A selection was made of the bundle where the filaments were parallel, and then the FFT function was run on that selection. The resulting power spectrum was trimmed based on guidance from Dr. Alexies Huet of the Conway lab to remove artifacts of the microscope, visible as a ring in the power spectrum (see Appendix B for detail on FFT). The trimmed data was used to generate an inverse FFT.

APPENDIX A

A.1 INVESTIGATION OF ROCK COILED-COIL REGION CONFORMATIONS

As mentioned in the introduction, Rock, phosphorylates non-muscle Myosin II leading to actin contractility [88]. This contraction of the actomyosin network is central to cell morphology in several developing structures. Rock is a parallel dimer consisting of N-terminal Kinase domains, central coiled-coil regions and C-terminal Plekstrin Homology (PH) and C1 domains [64, 65, 80, 83, 88]. The Dimerization domain is C-terminal to the Kinase domain [64]. Rock is believed to be inhibited through a direct interaction between the Kinase domain and PH/C1 domains (Fig. A1.1.) [80]. Within the coiled-coil region are two known binding domains, a Shroom Binding Domain (SBD) and RhoA Binding Domain (RBD) [72, 82, 86]. It has been shown that Rock is activated through the binding of RhoA GTPase to the RBD [83]. Work from the VanDemark lab suggests that binding of Shroom's SD2 to the SBD also can activate the Kinase. This interaction in the coiled-coil region is predicted to displace the PH/C1 domains from the kinase domain. In fact, displacement of the C-terminus of Rock, either by proteolysis, binding to lipids, or mutation, renders the Kinase constitutively active [72, 80, 83, 105-107].

While we understand how Rock can be activated, very little is known about the conformational changes that occur for Rock to achieve the inhibited state or active state. Solved structures of pieces of the coiled-coil region are all parallel coiled-coil dimers, with little

suggestion that they are able to bend [72, 82, 86, 87]. There has been no evidence for a hinge in the region. Based on these observations and hypotheses, my early work focused on trying to determine the possible conformations that Rock's coiled-coil region, as well as full-length Rock, is capable of adopting. The following describes my efforts to that end, using several different techniques.

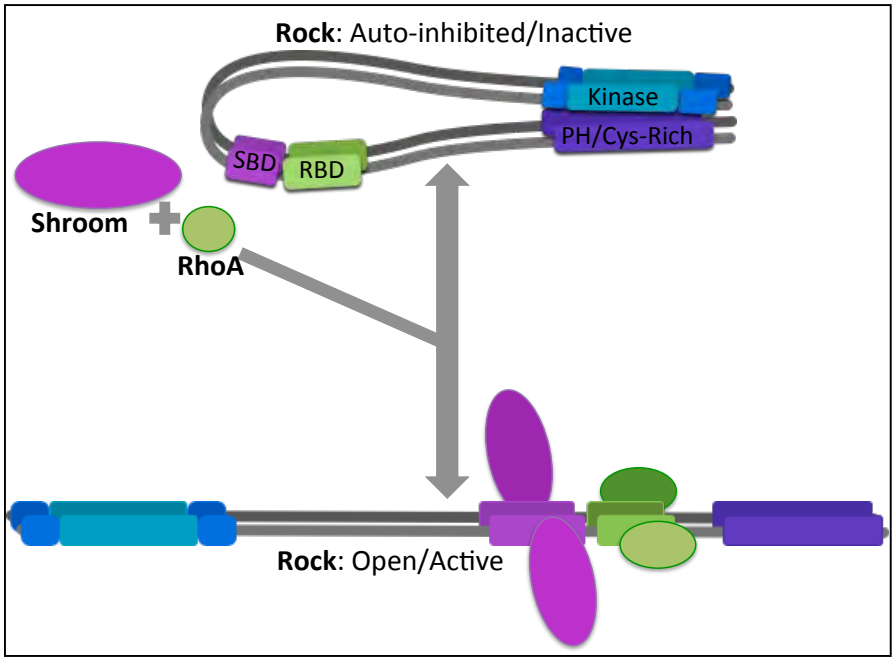

Figure A1.1: Model of Rock activation via binding of Shroom and/or RhoA.

Rock is inhibited through an interaction between the C-terminal PH/Cys-Rich domains and the Kinase domains. We believe this interaction is achieved through an intra-molecular interaction and not an inter-molecular interaction. Rock is activated by binding of Shroom or RhoA, possibly through steric hindrance of the closed conformation.

A.2 RESULTS AND DISSCUSION

A.2.1 Purification

After optimizing expression of the Rock coiled-coil proteins (6xHis-hRock1 436-1094 and GST-hRock1 593-1062), plasmids were transformed into the RosettaII *E. coli* expression cells. The additional tRNAs expressed by these bacteria increased total expression compared to that of BL21 or RIPL cells. Additionally, using freshly transformed cells to start a liquid overnight culture for auto-induction increased the total yield and 6 L overnight auto-inductions were necessary to yield sufficient protein (750µL of 11mg/mL from 6L). Later, for use with TEM, less total protein (final 5mLs of 1mg/mL) was needed and smaller growths were performed (1-2L).

After growing cultures for 24 hours at room temperature, the cells were collected by centrifugation at 6,000xg for 10 minutes. The cells were flash frozen and stored at -80°C or immediately resuspended to a concentration of 10 mg/ml of cells/Lysis buffer. The Lysis buffer used for 6xHis-hRock1 436-1094 was: 500mM NaCl, 25mM Tris, 5mM Imidazole, 1mM βME, at pH8 plus protease inhibitors Leupeptin, Pepstatin, Aprotinin and PMSF at 1:1000x ratios. The addition of these 4 protease inhibitors was necessary to reduce the degradation of the full-length protein (data not shown). The cells were lysed by homogenization with the Avestin Emulsiflex and soluble proteins were separated from insoluble cell matter by centrifugation at 12,500xg for 30 minutes at 4C.

The supernatant from 6xHis-Rock 436-1094 was passed over a Ni-sepharose gravity column. Several wash steps similar to those described in the Materials and Methods for the preparation of the Shroom SD1s were used. 6xHis-Rock 436-1094 was eluted from the column using Lysis buffer with 200mM Imidazole and fractions were assayed by SDS-PAGE to

determine yield and stability. Fractions containing 6xHis-Rock 436-1094 were treated with 6xHis-TEV protease, purified by the VanDemark Lab, for a minimum of 3 hour at room temperature while dialyzing into TEV buffer (500mM NaCl, 25mM Tris, 8% glycerol, pH 8.5). The cleaved protein was then run over a Ni-sepharose gravity column to separate the cleaved protein from the His tag and His-TEV. Flow through was collected and dialyzed into a 25mM Tris, 50mM NaCl, 2% glycerol, pH 8 buffer overnight at 4C. The dialyzed protein was then filtered, loaded onto an anion-exchange column, and eluted using an increasing gradient of NaCl in 25mM Tris, 2% glycerol at pH8. Typically, the desired protein eluted from the column at around 350-450 mM of NaCl. The fractions were analyzed by SDS-PAGE and Coomassie stain. Fractions containing the highest concentration of full-length protein were then concentrated to a volume around 3mL and loaded onto an S500 size exclusion chromatography column for final purification. The sample eluted off as a single peak. Given that Rock is a parallel dimer, it is likely that degradation products remain because they are part of a dimer. Final purification of Rock436-1094 can be seen in Fig. A1.2 lane 2.

GST-hRock1 593-1062 was resuspended in NETN (100mM NaCl, 20mM Tris pH8, .5mM EDTA, and .5% NP-40) buffer and purified in the same way as His-hRock1 436-1094, however the supernatant was passed over a gravity glutathione-sepharose column. Protein was eluted with NETN buffer containing 500mM glutathione. Eluted protein was dialyzed into the same low salt buffer as hRock1 436-1094 prior to anion-exchange chromatography. The GST-tag was not cleaved from the protein. Fractions were analyzed by SDS-PAGE and Coomassie stain. The fractions covering the center of the peak were collected and concentrated for further experiments. This protein was only used for TEM. Final purification of GST-hRock1 593-1062 can be seen in Fig. A1.2 Lane 1.

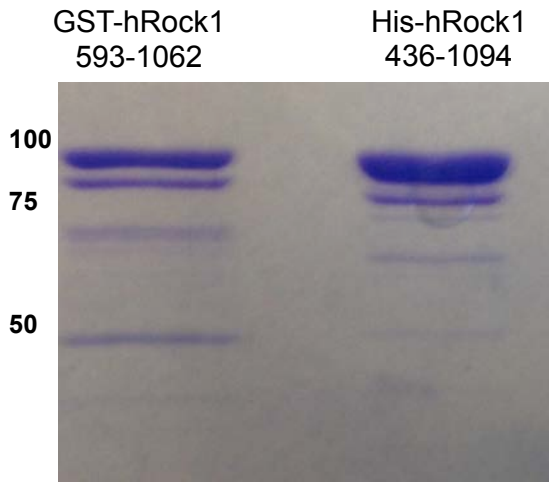

Figure A1.2: Purified hRock1 CC proteins used for these studies.

Both of these pieces of the Coiled-coil region of Rock degraded even in the presence of protease inhibitors during purification.

A.2.2 Crystallography

Once I had sufficiently pure protein samples of hRock1 436-1094, I proceeded with crystallization trials. I attempted to crystalize the protein in the 12 most common conditions used for solved PDB structures, as compiled by the VanDemark Lab. However, the proteins precipitated out of solution within 24 hours in most of the conditions tested. By 2 weeks there were still no crystals or promising hits from this range of crystallization buffers. In addition, I also tried two large commercial screens, Wizard II (Rigaku, SKU:1009531) and JCSG+ (Molecular Dimensions, MD1-37) . There were 3 potentially promising hits that were further examined by varying the ratios of precipitant, salt, and protein. However, none of these trials yielded suitable crystals. The conditions either precipitated the protein, yielded salt crystals, or remained clear even after 4 months. At this point, we abandoned crystallization as an option for understanding the structure of the entire coiled-coil region. Given our hypothesis that the coiled-

coil region is reasonably flexible, it is understandable that it might not form ordered crystals. For this reason, we explored alternate techniques for understanding the possible conformations of the Rock coiled-coil region.

A.2.3 Static Light Scattering

One way to determine if the coiled-coil region of Rock is indeed flexible would be to measure the average length of this region in solution. Therefore, I utilized the technique of Static Light Scattering (SLS) to accomplish this. This technique measures the angle of refraction of a laser directed at a sample in solution [108, 109]. This measurement can be translated into a Radius of gyration, which is approximately equal to the radius of the sphere created by a tumbling molecule in solution. This allows us to relate the Radius of gyration directly to the overall size of the molecule. If the coiled-coil region is mostly a long rod, rotating in all directions, I expect to observe a sphere in which the diameter is equal to the overall length of the molecule. Conversely, if the coiled-coil region can fold onto itself or is flexible, I would expect an average radius of gyration that is smaller then the predicted length of the linear coiled-coil.

When hRock1 463-1094 was subjected to this analysis at two concentrations (1mg/ml and 0.5mg/ml) I observed a range of radii that fit under a bell curve (Fig. A1.3). The bell curves of the replicates have similar minimums, maximums and peaks. The average minimum radius was approximately 10 nm and the maximum average was approximately 33 nm. Given the correlation to size of the molecule, hRock1 436-1094 is capable of achieving a conformation around 20 nm to 66 nm in length. This fits well with the maximum predicted size of this piece of the coiled-coil region of ~70nm. The measurements of SLS often under represent the actual size,

due to weak signal from the edges of a molecule [109]. The range of sizes measured as the coiled-coil region suggests it is a dynamic, flexible molecule, and not strictly linear or folded.

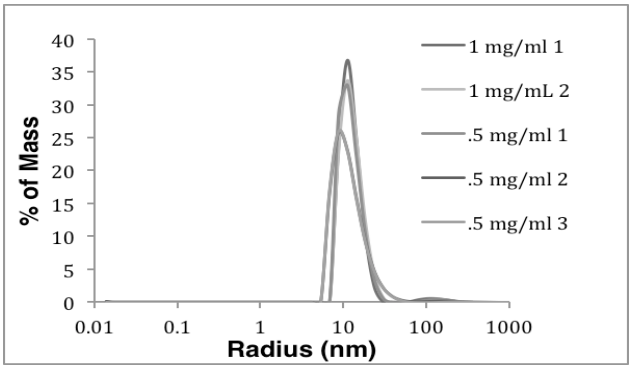

Figure A1.3: Static light Scattering of hRock1 436-1094.

Percent Mass of hRock1 coiled-coil 436-1094 at a given radius of gyration. At two different concentrations of Rock's coiled-coil representing the same range of possible diameters.

A.2.4 Small Angle X-Ray Scattering

Another technique that can be used to determine the shape of a molecule is Small Angle X-Ray Scattering (SAXS). SAXS utilizes similar principles as crystallography, in that diffraction data from x-rays is used to determine the location of atoms in a molecule [110-112]. However for SAXS a liquid solution is used, eliminating the need to crystalize. This seemed a possible alternative for the Rock coiled-coil region because we were having difficulty crystalizing the protein.

The SAXS machine at the Department of Structural Biology did not yield any usable data for a reconstruction due to the fact that the machine in question has a particularly weak X-Ray source. Due to the weak source it was difficult to get scattering data of any kind. I tried several times running samples of buffer alone as well as my sample of hRock1 436-1094 for either 7-

hour or 14-hour runs. Neither of these produced data that was trustworthy due to the lack of signal strength. Given these complications we proceeded with other techniques to visualize molecules of Rock.

A.2.5 Transmission Electron Microscopy

In my continued attempts to understand the conformation of the Rock coiled-coil region, I pursued Transmission Electron Microscopy (TEM). Grids were prepared in the same manner as described in the Materials and Methods for TEM grids of F-actin + Shroom SD1. Initially, I made grids using hRock1 436-1094. While I observed structures that could possibly be molecules of Rock, given their small size and the background signal it was impossible to make any conclusions from these grids (Fig. A1.4 A). I then made grids using the GST-hRock1 593-1062 in the hopes that the globular tag of GST would aid in visualization. The grids were also made with F-actin present to act as a staining control. While F-actin could be visualized, there were no molecules that were conclusively GST-hRock1 593-1062. The problem remained that it was difficult to tell the difference between background and molecules that were smaller than F-actin. Finally, I made grids of full-length hRock1 purified from MDCK cells by Jenna Zalewski. While there may have been some promising leads on the grids (Fig. A1.4 B), no conclusive data resulted. In summary, this procedure did not yield enough contrast to clearly visualize Rock.

A group recently published a composite structure for full-length Rock that they generated with TEM [81]. Rock is easily visualized in their images. The difference between my TEM attempts and theirs lies in the technique used in making the grids. Whereas I used a standard negative staining technique in which Uranyl Acetate is spotted on top of the sample, leading to reduced contrast, they utilized a low-angle shadowing technique [113]. This technique applies

carbon at a specific angle to the sample grid prior to negative staining. This increases the contrast, and is particularly useful in visualizing small molecules. If this work is pursued in the future, I believe attempting this technique will greatly increase our chances of visualizing single molecules of Rock.

Based on the sample image provided in their article, it appears that full-length Rock's coiled-coil region is not a straight rod, but that the coiled-coil region is flexible. While some molecules are fully extended, others were bent enough to bring the Kinase domains in close proximity to the PH/C1 domains. The range of conformations visible in the single image actually supports the idea that the coiled-coil region is flexible and allows dynamic interaction between the kinase domain and the C-terminus even though the authors say Rock is a ridged molecule.

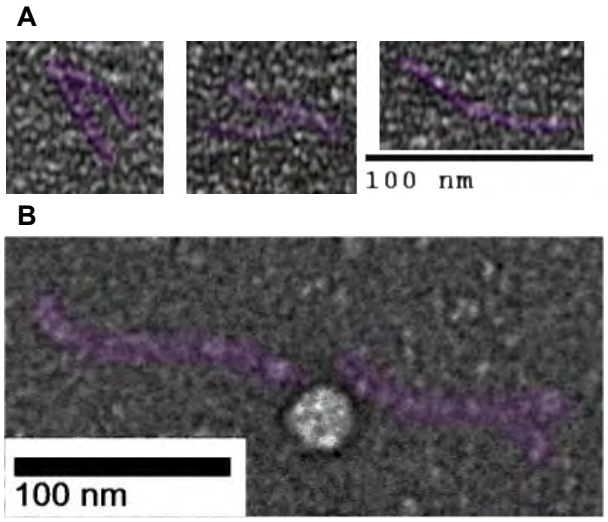

Figure A1.4: Inconclusive TEM of hRock1 Coiled-Coil and Full-Length protein.

A) hRock1 coiled-coil TEM, false colored to highlight what is potentially Rock B) hRock1 Full-Length, false colored.. Due to its small size, TEM, with conventional negative staining techniques, was inconclusive for both the coiled-coil region as well as full-length hRock1.

APPENDIX B

B.1 FOUIER TRANSFORM AND USE WHEN ANALYZING TEM

Fourier Transform (FT) allows for the conversion of an image into spatial data and helps to define a relationship between a projection (the image) and the original molecule. It is, in essence, a mathematical representation of the image. The output of a FT, similar to that of a diffraction pattern generated in x-ray crystallography, gives you information on the spacing of elements of an object. FT of EM images has been a method of data analysis since the 1960s [114]. If there is repetition in the distance between points, such as the cross over point in an actin filament that is 360Å apart, these compound to create an increased signal and form the power spectrum, which is the output of an FT of an image. Where these signals fall in the power spectrum are layer lines. Equation B1, derived by Sukow and DeRosier [94], explains that the FT of an actin raft, which is a flat actin bundle, is the summation of the FT of a single actin filament.

Equation B1: Fourier Transform of an Actin Raft

$$F(R,Z) = \sum_{k}\sum_{i}\sum_{n} G_n(R,Z_i)e^{i\left(2\pi R x_k - 2\pi Z_i z_k - n\phi_k\right)}$$

This filament is defined as centered at the location x_k and z_k, with rotation ϕ_k . "G_n is the radial dependence of the nth order component of the lth layer line. Z_l is the axial position of the lth layer line and k is an integer which denotes the index of the filament and the raft" [115].

With the theory of utilizing FT to analyze actin and actin bundles/rafts established, image processing software, ImageJ ((NIH, Bethesda, MD, USA) contains a function that will perform a discrete Fourier Transform of images, known as a Fast Fourier Transform (FFT) as well as the inverse (inverse FFT) that allows a simple FT to be done on a selection of an image defined by the user. FFT is done to determine if multiple images can be compiled to build a reconstruction. Images can only be compiled if their FFT are similar, which would mean that the helical pitch and spacing of filaments are the same. Determining that the actin filaments are in the same orientation and that the spacing of the turns of the helix are the same are critical to an eventual reconstruction. While performing TEM, there are often artifacts from the microscope that affect the signal and background. Data trimming can help to remove these artifacts, however, you can lose some information in doing so. For example, the TEM often produces a signal that can be seen in the power spectrum of the FFT as a ring. FFT can be trimmed to remove these data points and those from resolutions not truly achievable by TEM (better than 6Å). If the power spectrums from multiple filaments or bundles are the same, the images can be used to begin to compile a 3D reconstruction [94, 98, 116, 117].

The power spectrum can also be reinterpreted into an image, an inverse FFT. If your molecule has genuine structural repeats, they will appear in the inverse FFT as well. If your inverse FFT is similar to that of the original image it leads credence to the information you are compiling on your structure. Measurements of spacing of the repeats, or filament spacing can be made from these inverse images.

BIBLOGRAPHY

1. McNeill, H., *Planar cell polarity: keeping hairs straight is not so simple.* Cold Spring Harb Perspect Biol, 2010. **2**(2): p. a003376.
2. McGreevy, E.M., et al., *Shroom3 functions downstream of planar cell polarity to regulate myosin II distribution and cellular organization during neural tube closure.* Biol Open, 2015. **4**(2): p. 186-96.
3. Ossipova, O., et al., *Role of Rab11 in planar cell polarity and apical constriction during vertebrate neural tube closure.* Nat Commun, 2014. **5**: p. 3734.
4. Wang, J., et al., *Dishevelled genes mediate a conserved mammalian PCP pathway to regulate convergent extension during neurulation.* Development, 2006. **133**(9): p. 1767-78.
5. Wang, M., et al., *Role of the planar cell polarity gene Protein tyrosine kinase 7 in neural tube defects in humans.* Birth Defects Res A Clin Mol Teratol, 2015. **103**(12): p. 1021-7.
6. Hildebrand, J.D., *Shroom regulates epithelial cell shape via the apical positioning of an actomyosin network.* J Cell Sci, 2005. **118**(Pt 22): p. 5191-203.
7. Nishimura, T., H. Honda, and M. Takeichi, *Planar cell polarity links axes of spatial dynamics in neural-tube closure.* Cell, 2012. **149**(5): p. 1084-97.
8. Plageman, T.F., Jr., et al., *Pax6-dependent Shroom3 expression regulates apical constriction during lens placode invagination.* Development, 2010. **137**(3): p. 405-15.
9. Zhou, J., et al., *Force production and mechanical accommodation during convergent extension.* Development, 2015. **142**(4): p. 692-701.
10. Claessens, M.M., et al., *Actin-binding proteins sensitively mediate F-actin bundle stiffness.* Nat Mater, 2006. **5**(9): p. 748-53.
11. De La Cruz, E.M. and M.L. Gardel, *Actin Mechanics and Fragmentation.* J Biol Chem, 2015. **290**(28): p. 17137-44.
12. Galkin, V.E., et al., *Near-atomic resolution for one state of F-actin.* Structure, 2015. **23**(1): p. 173-82.
13. Gurung, R., et al., *Actin polymerization is stimulated by actin cross-linking protein palladin.* Biochem J, 2016. **473**(4): p. 383-96.
14. Heisenberg, C.P. and Y. Bellaiche, *Forces in tissue morphogenesis and patterning.* Cell, 2013. **153**(5): p. 948-62.
15. Holmes, K.C., et al., *Atomic model of the actin filament.* Nature, 1990. **347**(6288): p. 44-9.
16. Kabsch, W., et al., *Atomic structure of the actin:DNase I complex.* Nature, 1990. **347**(6288): p. 37-44.

17. Kudryashov, D.S., et al., *The crystal structure of a cross-linked actin dimer suggests a detailed molecular interface in F-actin.* Proc Natl Acad Sci U S A, 2005. **102**(37): p. 13105-10.
18. Murrell, M., et al., *Forcing cells into shape: the mechanics of actomyosin contractility.* Nat Rev Mol Cell Biol, 2015. **16**(8): p. 486-98.
19. Reutzel, R., et al., *Actin crystal dynamics: structural implications for F-actin nucleation, polymerization, and branching mediated by the anti-parallel dimer.* J Struct Biol, 2004. **146**(3): p. 291-301.
20. Oda, T., et al., *The nature of the globular- to fibrous-actin transition.* Nature, 2009. **457**(7228): p. 441-5.
21. Bretscher, A., *Fimbrin is a cytoskeletal protein that crosslinks F-actin in vitro.* Proceedings of the National Academy of …, 1981.
22. dos Remedios, C.G., et al., *Actin binding proteins: regulation of cytoskeletal microfilaments.* Physiol Rev, 2003. **83**(2): p. 433-73.
23. Galkin, V.E., et al., *High-resolution cryo-EM structure of the F-actin-fimbrin/plastin ABD2 complex.* Proc Natl Acad Sci U S A, 2008. **105**(5): p. 1494-8.
24. George, S.P., et al., *Dimerization and actin-bundling properties of villin and its role in the assembly of epithelial cell brush borders.* J Biol Chem, 2007. **282**(36): p. 26528-41.
25. Klein, M.G., et al., *Structure of the actin crosslinking core of fimbrin.* Structure, 2004. **12**(6): p. 999-1013.
26. Pelletier, O., et al., *Structure of actin cross-linked with alpha-actinin: a network of bundles.* Phys Rev Lett, 2003. **91**(14): p. 148102.
27. Uribe, R. and D. Jay, *A review of actin binding proteins: new perspectives.* Mol Biol Rep, 2009. **36**(1): p. 121-5.
28. Medeiros, N.A., D.T. Burnette, and P. Forscher, *Myosin II functions in actin-bundle turnover in neuronal growth cones.* Nat Cell Biol, 2006. **8**(3): p. 215-26.
29. Udovichenko, I.P., D. Gibbs, and D.S. Williams, *Actin-based motor properties of native myosin VIIa.* J Cell Sci, 2002. **115**(Pt 2): p. 445-50.
30. Alborghetti, M.R., et al., *Structural analysis of intermolecular interactions in the kinesin adaptor complex fasciculation and elongation protein zeta 1/ short coiled-coil protein (FEZ1/SCOCO).* PloS one, 2013. **8**(10).
31. Banerjee, J., C.C. Fischer, and P.B. Wedegaertner, *The amino acid motif L/IIxxFE defines a novel actin-binding sequence in PDZ-RhoGEF.* Biochemistry, 2009. **48**(33): p. 8032-43.
32. Machaidze, G., et al., *Actin filament bundling and different nucleating effects of mouse Diaphanous-related formin FH2 domains on actin/ADF and actin/cofilin complexes.* J Mol Biol, 2010. **403**(4): p. 529-45.
33. Takenawa, T. and S. Suetsugu, *The WASP-WAVE protein network: connecting the membrane to the cytoskeleton.* Nat Rev Mol Cell Biol, 2007. **8**(1): p. 37-48.
34. Machesky, L.M. and K.L. Gould, *The Arp2/3 complex: a multifunctional actin organizer.* Curr Opin Cell Biol, 1999. **11**(1): p. 117-21.
35. Machesky, L.M. and R.H. Insall, *Scar1 and the related Wiskott–Aldrich syndrome protein, WASP, regulate the actin cytoskeleton through the Arp2/3 complex.* Current biology, 1998.

36. Mullins, R.D., J.A. Heuser, and T.D. Pollard, *The interaction of Arp2/3 complex with actin: nucleation, high affinity pointed end capping, and formation of branching networks of filaments.* Proc Natl Acad Sci U S A, 1998. **95**(11): p. 6181-6.
37. Robinson, R.C., et al., *Crystal structure of Arp2/3 complex.* Science, 2001. **294**(5547): p. 1679-84.
38. Yarar, D., et al., *The Wiskott-Aldrich syndrome protein directs actin-based motility by stimulating actin nucleation with the Arp2/3 complex.* Curr Biol, 1999. **9**(10): p. 555-8.
39. Kim, L.Y., et al., *The Structural Basis of Actin Organization by Vinculin and Metavinculin.* J Mol Biol, 2016. **428**(1): p. 10-25.
40. Meng, J., et al., *High-resolution crystal structures of villin headpiece and mutants with reduced F-actin binding activity.* Biochemistry, 2005. **44**(36): p. 11963-73.
41. Friederich, E., et al., *Villin function in the organization of the actin cytoskeleton. Correlation of in vivo effects to its biochemical activities in vitro.* J Biol Chem, 1999. **274**(38): p. 26751-60.
42. Siedlik, M.J. and C.M. Nelson, *Regulation of tissue morphodynamics: an important role for actomyosin contractility.* Curr Opin Genet Dev, 2015. **32**: p. 80-5.
43. Hammer, J.A. and J.R. Sellers, *Walking to work: roles for class V myosins as cargo transporters.* Nat Rev Mol Cell Biol, 2012. **13**(1): p. 13-26.
44. Hartman, M.A. and J.A. Spudich, *The myosin superfamily at a glance.* J Cell Sci, 2012. **125**(Pt 7): p. 1627-32.
45. Mehta, A.D., et al., *Myosin-V is a processive actin-based motor.* Nature, 1999. **400**(6744): p. 590-593.
46. von der Ecken, J., et al., *Structure of the F-actin-tropomyosin complex.* Nature, 2015. **519**(7541): p. 114-7.
47. Drees, F., et al., *α-catenin is a molecular switch that binds E-cadherin-β-catenin and regulates actin-filament assembly.* Cell, 2005.
48. Hartsock, A. and W.J. Nelson, *Adherens and tight junctions: structure, function and connections to the actin cytoskeleton.* Biochim Biophys Acta, 2008. **1778**(3): p. 660-9.
49. Rimm, D.L., E.R. Koslov, and P. Kebriaei, *Alpha 1 (E)-catenin is an actin-binding and-bundling protein mediating the attachment of F-actin to the membrane adhesion complex.* Proceedings of the …, 1995.
50. Yamada, S., et al., *Deconstructing the cadherin-catenin-actin complex.* Cell, 2005. **123**(5): p. 889-901.
51. Amano, M., et al., *Formation of actin stress fibers and focal adhesions enhanced by Rho-kinase.* Science, 1997.
52. Insall, R.H. and L.M. Machesky, *Actin dynamics at the leading edge: from simple machinery to complex networks.* Dev Cell, 2009. **17**(3): p. 310-22.
53. Plageman, T.F., Jr., et al., *A Trio-RhoA-Shroom3 pathway is required for apical constriction and epithelial invagination.* Development, 2011. **138**(23): p. 5177-88.
54. Simoes Sde, M., A. Mainieri, and J.A. Zallen, *Rho GTPase and Shroom direct planar polarized actomyosin contractility during convergent extension.* J Cell Biol, 2014. **204**(4): p. 575-89.
55. Dye, D.E., et al., *hShroom1 links a membrane bound protein to the actin cytoskeleton.* Cell Mol Life Sci, 2009. **66**(4): p. 681-96.

56. Elliott, H., et al., *Myosin II controls cellular branching morphogenesis and migration in three dimensions by minimizing cell-surface curvature.* Nat Cell Biol, 2015. **17**(2): p. 137-47.
57. Etournay, R., et al., *Shroom2, a myosin-VIIa- and actin-binding protein, directly interacts with ZO-1 at tight junctions.* J Cell Sci, 2007. **120**(Pt 16): p. 2838-50.
58. Fairbank, P.D., et al., *Shroom2 (APXL) regulates melanosome biogenesis and localization in the retinal pigment epithelium.* Development, 2006. **133**(20): p. 4109-18.
59. Farber, M.J., R. Rizaldy, and J.D. Hildebrand, *Shroom2 regulates contractility to control endothelial morphogenesis.* Mol Biol Cell, 2011. **22**(6): p. 795-805.
60. Lee, C., M.P. Le, and J.B. Wallingford, *The shroom family proteins play broad roles in the morphogenesis of thickened epithelial sheets.* Dev Dyn, 2009. **238**(6): p. 1480-91.
61. Plageman, T.F., Jr., et al., *Shroom3 and a Pitx2-N-cadherin pathway function cooperatively to generate asymmetric cell shape changes during gut morphogenesis.* Dev Biol, 2011. **357**(1): p. 227-34.
62. Yoder, M. and J.D. Hildebrand, *Shroom4 (Kiaa1202) is an actin-associated protein implicated in cytoskeletal organization.* Cell Motil Cytoskeleton, 2007. **64**(1): p. 49-63.
63. Nishimura, T. and M. Takeichi, *Shroom3-mediated recruitment of Rho kinases to the apical cell junctions regulates epithelial and neuroepithelial planar remodeling.* Development, 2008. **135**(8): p. 1493-502.
64. Leung, T., et al., *The p160 RhoA-binding kinase ROK alpha is a member of a kinase family and is involved in the reorganization of the cytoskeleton.* Molecular and cellular biology, 1996. **16**(10): p. 5313-5327.
65. Matsui, T., et al., *Rho-associated kinase, a novel serine/threonine kinase, as a putative target for small GTP binding protein Rho.* The EMBO journal, 1996. **15**(9): p. 2208-2216.
66. Munjal, A., et al., *A self-organized biomechanical network drives shape changes during tissue morphogenesis.* Nature, 2015. **524**(7565): p. 351-5.
67. Bolinger, C., et al., *Specific isoforms of drosophila shroom define spatial requirements for the induction of apical constriction.* Dev Dyn, 2010. **239**(7): p. 2078-93.
68. Dietz, M.L., et al., *Differential actin-dependent localization modulates the evolutionarily conserved activity of Shroom family proteins.* J Biol Chem, 2006. **281**(29): p. 20542-54.
69. Hildebrand, J.a.S., P., *Shroom, a PDZ Domain-Containing Actin-Binding Protein, is Resquired for Neural Tube Morphogenesis in Mice.* Cell, 1999. **99**.
70. Mohan, S., et al., *Structure of Shroom domain 2 reveals a three-segmented coiled-coil required for dimerization, Rock binding, and apical constriction.* Mol Biol Cell, 2012. **23**(11): p. 2131-42.
71. Das, D., et al., *The interaction between Shroom3 and Rho-kinase is required for neural tube morphogenesis in mice.* Biol Open, 2014. **3**(9): p. 850-60.
72. Mohan, S., et al., *Structure of a highly conserved domain of Rock1 required for Shroom-mediated regulation of cell morphology.* PLoS One, 2013. **8**(12): p. e81075.
73. *Solution structure of the PDZ domain from human Shroom family member 4, PDB.* Unpublished.
74. Bezprozvanny, I. and A. Maximov, *Classification of PDZ domains.* FEBS Lett, 2001. **509**(3): p. 457-62.
75. Kalyoncu, S., O. Keskin, and A. Gursoy, *Interaction prediction and classification of PDZ domains.* BMC Bioinformatics, 2010. **11**: p. 357.

76. Dickson, H.M., et al., *Targeted inhibition of the Shroom3-Rho kinase protein-protein interaction circumvents Nogo66 to promote axon outgrowth.* BMC Neurosci, 2015. **16**: p. 34.
77. Dickson, H.M., et al., *POSH is an intracellular signal transducer for the axon outgrowth inhibitor Nogo66.* J Neurosci, 2010. **30**(40): p. 13319-25.
78. Hagens, O., et al., *A new standard nomenclature for proteins related to Apx and Shroom.* BMC Cell Biol, 2006. **7**: p. 18.
79. Hagens, O., et al., *Disruptions of the novel KIAA1202 gene are associated with X-linked mental retardation.* Hum Genet, 2006. **118**(5): p. 578-90.
80. Amano, M., et al., *The COOH terminus of Rho-kinase negatively regulates rho-kinase activity.* J Biol Chem, 1999. **274**(45): p. 32418-24.
81. Truebestein, L., et al., *A molecular ruler regulates cytoskeletal remodelling by the Rho kinases.* Nat Commun, 2015. **6**: p. 10029.
82. Dvorsky, R., et al., *Structural insights into the interaction of ROCKI with the switch regions of RhoA.* J Biol Chem, 2004. **279**(8): p. 7098-104.
83. Ishizaki, T., et al., *The small GTP-binding protein Rho binds to and activates a 160 kDa Ser/Thr protein kinase homologous to myotonic dystrophy kinase.* EMBO J, 1996. **15**(8): p. 1885-93.
84. Jacobs, M., et al., *The structure of dimeric ROCK I reveals the mechanism for ligand selectivity.* J Biol Chem, 2006. **281**(1): p. 260-8.
85. Maesaki, R., et al., *The structural basis of Rho effector recognition revealed by the crystal structure of human RhoA complexed with the effector domain of PKN/PRK1.* Mol Cell, 1999. **4**(5): p. 793-803.
86. Shimizu, T., et al., *Parallel coiled-coil association of the RhoA-binding domain in Rho-kinase.* J Biol Chem, 2003. **278**(46): p. 46046-51.
87. Tu, D., et al., *Crystal structure of a coiled-coil domain from human ROCK I.* PLoS One, 2011. **6**(3): p. e18080.
88. Amano, M., et al., *Phosphorylation and activation of myosin by Rho-associated kinase (Rho-kinase).* J Biol Chem, 1996. **271**(34): p. 20246-9.
89. Escuin, S., et al., *Rho-kinase-dependent actin turnover and actomyosin disassembly are necessary for mouse spinal neural tube closure.* J Cell Sci, 2015. **128**(14): p. 2468-81.
90. Haigo, S.L., et al., *Shroom Induces Apical Constriction and Is Required for Hingepoint Formation during Neural Tube Closure.* Current Biology, 2003. **13**(24): p. 2125-2137.
91. Studier, F.W., *Protein production by auto-induction in high density shaking cultures.* Protein Expr Purif, 2005. **41**(1): p. 207-34.
92. Srivastava, J. and D. Barber, *Actin co-sedimentation assay; for the analysis of protein binding to F-actin.* J Vis Exp, 2008(13).
93. Scatchard, G., *The Attractions of Proteins for Small Molecules and Ions.* Annals of the New York Academy of Sciences, 1949. **51**(4): p. 660-672.
94. Catherine Sukow, D.D., *How to Analyze Electron Micrographs of Rafts of Actin Filametns Crosslinked by Actin-binding Proteins.* Journal of Molecular Biology, 1998.
95. Galkin, V.E., et al., *Structural polymorphism in F-actin.* Nat Struct Mol Biol, 2010. **17**(11): p. 1318-23.
96. Ito, T., et al., *Electron microscopic visualization of the filament binding mode of actin-binding proteins.* J Mol Biol, 2011. **408**(1): p. 26-39.

97. Brown, J.W. and C.J. McKnight, *Molecular model of the microvillar cytoskeleton and organization of the brush border.* PLoS One, 2010. **5**(2): p. e9406.
98. Bullitt, E.S., et al., *Three-dimensional reconstruction of an actin bundle.* J Cell Biol, 1988. **107**(2): p. 597-611.
99. Volkmann, N., et al., *An atomic model of actin filaments cross-linked by fimbrin and its implications for bundle assembly and function.* J Cell Biol, 2001. **153**(5): p. 947-56.
100. Pollard, T.D. and J.A. Cooper, *Actin and actin-binding proteins. A critical evaluation of mechanisms and functions.* Annu Rev Biochem, 1986. **55**(1): p. 987-1035.
101. Li, J., et al., *Ezrin controls the macromolecular complexes formed between an adapter protein Na+/H+ exchanger regulatory factor and the cystic fibrosis transmembrane conductance regulator.* J Biol Chem, 2005. **280**(45): p. 37634-43.
102. Plasmid developed in the Van Demark Lab at the University of Pittsburgh. Unpublished
103. Plasmid developed in the Van Demark Lab at the University of Pittsburgh. Unpublished
104. Jansen, S., et al., *Mechanism of actin filament bundling by fascin.* J Biol Chem, 2011. **286**(34): p. 30087-96.
105. Araki, S., et al., *Arachidonic acid-induced Ca2+ sensitization of smooth muscle contraction through activation of Rho-kinase.* Pflügers Archiv, 2000. **441**(5): p. 596-603.
106. Isaka, N., et al., *Rho-associated kinase of chicken gizzard smooth muscle.* Journal of Biological …, 1999.
107. Yamaguchi, H., et al., *Molecular mechanism for the regulation of rho-kinase by dimerization and its inhibition by fasudil.* Structure, 2006. **14**(3): p. 589-600.
108. Berne, B.J. and R. Pecora, *Dynamic light scattering: with applications to chemistry, biology, and physics.* Dynamic light scattering: with applications to chemistry, biology, and physics, 1976.
109. Takagi, T., *Application of low-angle laser light scattering detection in the field of biochemistry: review of recent progress.* Journal of Chromatography A, 1990.
110. Hura, G.L., et al., *Robust, high-throughput solution structural analyses by small angle X-ray scattering (SAXS).* Nat Methods, 2009. **6**(8): p. 606-12.
111. Jacques, D.A. and J. Trewhella, *Small-angle scattering for structural biology--expanding the frontier while avoiding the pitfalls.* Protein Sci, 2010. **19**(4): p. 642-57.
112. Lipfert, J. and S. Doniach, *Small-angle X-ray scattering from RNA, proteins, and protein complexes.* Annu Rev Biophys Biomol Struct, 2007. **36**: p. 307-27.
113. Hendricks, G.M., *Metal shadowing for electron microscopy.* Methods Mol Biol, 2014. **1117**: p. 73-93.
114. De Rosier, D.J. and A. Klug, *Reconstruction of three dimensional structures from electron micrographs.* Nature, 1968. **217**(5124): p. 130-4.
115. Sukow, C. and D. DeRosier, *How to analyze electron micrographs of rafts of actin filaments crosslinked by actin-binding proteins.* J Mol Biol, 1998. **284**(4): p. 1039-50.
116. DeRosier, D.J. and L.G. Tilney, *How actin filaments pack into bundles.* Cold Spring Harbor symposia on …, 1982.
117. Egelman, E.H. and D.J. DeRosier, *The Fourier transform of actin and other helical systems with cumulative random angular disorder.* Acta Crystallographica Section A: …, 1982.